www.springer.com/41230
https://doi.org/10.1007/s41230-025-5013-1
Special Review CHINA FOUNDRY
Vol. 23 No. 2 March 2026

A review of sliver defects in Ni-based single crystal superalloys

***Sobhan Rajabinejad[1], Javad Yazdani[1], Majid Fouladvand[2], and Mohammad-Reza Ahmadpour Yazdi[3]**

1. Department of Materials Engineering, Malek Ashtar University of Technology, Tehran, Iran

2. Department of Industrial Engineering, University of Bologna, Italy

3. Department of Materials Science and Engineering, Sharif University of Technology, Tehran, Iran

Abstract: Sliver defects are a group of low-to-medium angle misoriented grains in Ni-based single crystal superalloys that have received more attention in recent years. Occurrence of these defects can negatively affect the mechanical properties of single crystal components. Therefore, studying the mechanisms of sliver formation and its effects on the final properties of alloys is of great importance. In this article, recent studies on the sliver defects were reviewed. Accordingly, the mechanisms of sliver formation as well as factors contributing to sliver initiation were studied. Additionally, effects of slivers on the mechanical properties of single crystal superalloys were discussed. Dendrite deformation and dendrite fracture are the main mechanisms for the sliver formation. This is a consequence of local stress concentration on dendrites during solidification. Therefore, locations such as inclusions, pores, geometrically complex areas, mould walls, freckle channels, etc. can be considered as the potential factors that promote the sliver initiation. Sliver formation significantly degrades the creep life of single-crystal superalloys. Studies have shown that when crystallographic misorientation exceeds approximately 15°, creep life can be reduced by up to 47%. Despite the absence of a standardized criterion for predicting or preventing sliver initiation and propagation, their occurrence can be minimized through optimization of solidification parameters, careful grain selection, proper casting geometry design, and rigorous control of material purity and equipment conditions.

Keywords: sliver; single crystal superalloy; misorientation; dendrite fracture; dendrite deformation; mechanical properties

CLC numbers: TG146.1+5 **Document code:** A **Article ID:** 1672-6421(2026)02-139-19

1 Introduction

Nickel-based superalloys are extensively used in high-temperature components of jet engines and industrial gas turbines[1-6]. Advancements in directional solidification (DS) technology, along with the successful manufacturing of columnar grain (CG) and single crystal (SC) superalloys, have contributed to substantial enhancements in their mechanical performance[7-11]. Despite recent advances in the field of CG and SC superalloys, there are always some challenges in their manufacturing processes. One of these challenges is the presence of solidification defects in DS superalloy parts. Porosities, microsegregation, misoriented or stray grains, high/low angle grain boundaries, freckles, slivers, and so on, can be considered as the solidification defects[12-20].

Micropores or microporosities are a group of solidification defects that impact the ultimate performance of cast alloys. Microporosities can develop from shrinkage and gas release during solidification process. By utilizing the advanced vacuum technology, gas porosities can be avoided during remelting and casting process. Hence, it can be concluded that the microporosities are mainly owing to solidification shrinkage[21]. Many investigations have been conducted to eliminate or reduce porosity in DS superalloys. For example, hot isostatic pressing (HIP) process can efficiently decrease the solidification microporosities, and therefore, enhance the mechanical properties of the cast superalloys[22-25]. In addition, Chen et al.[21] found that minor additions of carbon and hafnium into the SC superalloys has an advantageous influence on the alleviation of microshrinkage. This was typically resulted from the formation of MC carbides in the interdendritic regions, which counteracted volume

***Sobhan Rajabinejad**

M. Sc in materials engineering. He has 5 years experiences in steel industry.

E-mail: sobhanrajabinejad93@yahoo.com

Received: 2025-01-17; Revised: 2025-05-01; Accepted: 2025-05-29

shrinkage by inducing lattice expansion during the final stage of solidification.

The segregation of alloying elements is another kind of solidification defects in the cast superalloys. Local variation of alloy properties as well as occurrence of unfavorable phases, such as topologically closed packed (TCP) phases, are some of the deleterious effects on segregation. Therefore, Ni-based superalloys are mainly subjected to the solution heat treatment to remove microsegregation. Subsequently, the aging heat treatment are performed to regulate the size and morphology of γ′ phase[26-29]. In addition, with the development of new techniques for manufacturing DS superalloys, such as liquid metal cooling (LMC) technique[10, 30-35], downward directional solidification[36-39], and additive manufacturing (AM)[40-42], the detrimental effects of segregation can be reduced.

Freckles are usually resulted from dendrite fragmentation. Local remelting of dendrites and double diffusive convection in interdendritic channels are the main driving factors for dendrite fragmentation. This is a result of inverse density of the liquid metal in the mushy zone. These macroscale grain defects are one of the most critical factors for rejection of DS superalloy components. They can be seen as elongated chains of equiaxed grains, arranging almost parallel to the gravity direction[16, 43]. Various factors such as chemical composition and segregation of alloying elements[44-46], thermal gradient[35], withdrawal rate[37, 47, 48], withdrawal direction (upward or downward directional solidification)[37, 39], and geometrical parameters[49-53] can affect the formation and evolution of freckles.

Stray and misoriented grains are also a group of solidification defects in SC superalloys. Many studies have been conducted on the mechanism of their formation. According to the literature, many factors are involved in the formation of these defects[14, 54-56]. However, by optimizing the process parameters such as thermal gradient[56, 57], withdrawal rate of the mould[32, 55, 58-60], and geometrical factors[54, 61, 62], stray grains formation can be prevented to some extent.

Compared to the solidification defects mentioned above, slivers have received less attention in the literature. This may be due to the lower sensitivity of superalloy components to slivers compared to the other defects. However, recently, some studies[17, 63-71] have been conducted on the mechanism of sliver formation during solidification of SC superalloys. It should be noted that all the mentioned studies were conducted in recent years. In most of these works, numerical simulations were carried out alongside experimental investigations. This article provides a review of recent research on the sliver formation mechanism during directional solidification and its impact on the properties of SC superalloys.

2 History of research on sliver defects

In 1997, Beech et al.[72] appear to have been the first researchers to conduct a systematic investigation of sliver defects. They suggested that these defects are more likely to form on the reduced side of the cross-section, and proposed that this phenomenon could be associated with the presence of oxide residues. Al-Jarba et al.[73], in 2004, studied the influence of carbon addition on the cast structure and the formation of casting defects, including freckles, low-angle boundaries (LABs), high-angle boundaries (HABs), as well as slivers. According to their findings, the presence of slivers is not linked to thermal solutal convection, and addition of carbon is not an effective way to avoid these defects. Then, in 2013, Shi et al.[17] conducted a research on the mechanism of sliver formation in single crystal superalloys. They suggested that slivers commonly arose from defects at the inner surface of ceramic moulds. At the same time, a similar study was conducted by Aveson et al[74]. The samples with differing geometries were systematically studied using finite element analysis (FEM) and microstructural examination. Two potential sources of sliver defects were examined: (1) the dendrite fragmentation/detachment, or heterogeneous nucleation of sliver grains from the mould wall or oxide layer at the interface of the seed melt back; (2) dendrite deformation. It was found that sliver grains do not originate from dendrite fragmentation or conventional nucleation mechanisms. Instead, observations revealed that slivers predominantly form in regions where primary dendrites converge at the mould wall. Notably, slivers were rarely observed when the growth of primary dendrites diverged from the mould wall. This was rationalized by considering the bending moments and torques generated on primary and secondary dendrites caused by converging or diverging dendrites at the mould wall and their impact on competitive growth.

In 2018, Huo et al.[67] investigated the formation of slivers in the rejoined (extended) cross-section platforms of single crystal superalloys. While confirming the results of Ref. [74] regarding the necessity of dendrite deformation (bending and torsion) for sliver formation, the study identified three additional factors that may influence the continuous evolution of slivers within extended cross-section platforms: (1) a favorable orientation to compete with the neighboring dendrites; (2) appropriate local thermal conditions for continuous growth; and (3) an adequate space for dendrites to grow in three dimensions. Moreover, in 2019, some studies[66, 69] were conducted on the formation mechanism of slivers. Sun et al.[66] examined the lateral slivers formation in the platform area of single crystal turbine blades. They found that misorientation between neighboring sliver grains was restricted to a medium-angle range (10.5°). In addition, the lateral slivers occurred more frequently at lower withdrawal rates. The high stresses at the boundary between the blade body and platform area were identified as the cause of the lateral sliver defects based on the evolution of thermal profile and stress contours. Ma et al.[69] proposed that the sliver grains originated from the tearing of the dendrite stems that already existed in the mushy zone. The tearing of dendrite stems (arms) may be resulted from the mould wall adhesion that constrains the columnar dendrite shrinkage on the blade surface. Oxide residues are the second reason for dendrite tearing and they significantly affect the strength of dendrite stems. It seems that the results of Ma's research[69] are in contradiction with some

previous research works[66, 67, 74]. They proposed that the primary mechanism of sliver formation is dendritic deformation, and did not consider dendrite fragmentation, detachment, or tearing to play a role in the process. Nevertheless, Ma et al.[69] pointed out that the adjacent columnar dendrites support each other and limit the tilting of the broken dendrites. As a result, it can be said that most researchers are unanimous on the low-to-medium angle nature of slivers.

Since 2020, more studies related to the slivers have been continued[63-65, 68, 71, 75-77]. Xu et al.[63] and Huang et al.[68] determined the range of misorientation angle of the slivers to be 3.2°–12° and 3.5°–9.8°, respectivey. Xu et al.[63] reported that dendrite fragmentation occurs instead of undergoing significant plastic deformation. Huang et al.[64] also reported that the thermal contraction forces play a significant role in generation of sliver grains, in contrast to the interdendritic fluid flow. Han et al.[65] investigated the elongation and overgrowth of slivers, as well as the evolutionary mechanism by which freckles develop into sliver defects. Their measurements revealed that due to thermal stress induced by solidification shrinkage of the liquid with a high solute content, the dendrite deformation occurs specifically in the freckle channel, rather than in the single crystal area. Therefore, it can be concluded that the freckles formed during directional solidification of superalloys can also affect the formation of slivers. In 2023, Xia et al.[71] indicated that when the solid fraction in a cross-section exceeds a critical threshold, the structural constraints imposed by adjacent dendrites prevent the formation of large-angle slivers, even if individual dendrites fracture. It was recommended that the estimated minimum solid fraction of the cross-section should be approximately 79%, and this figure will remain constant despite any thermal gradients. In another research conducted in 2023, Yang et al.[75] studied the sliver formation mechanism in the C-shaped grain selectors during directional solidification of a single crystal superalloy. They reported that sliver initiation occurs during the final stage of solidification, primarily in regions of grain selection where high thermal stresses accumulate. In a recent study in 2024, Yu et al.[76] investigated the creep failure mechanism of sliver defects in a CMSX-4 single crystal superalloy. The results revealed a significant detrimental effect of slivers on the creep performance of single-crystal superalloys, with a 26.37% reduction in creep rupture life observed in samples containing slivers compared to defect-free counterparts. Fracture analysis showed that slivers primarily contribute to performance deterioration by promoting the extension of grain boundary microcracks through grain boundary sliding during the creep process, accelerating sample fracture. Utilizing crystal plasticity theory, they also suggested that for CMSX-4 alloy, the orientation of slivers should be restricted to within 8°. The latest relevant research has been conducted by Zhang et al[77]. They studied the evolution of sliver morphology in large-sized single-crystal superalloy blades. According to their experimental and simulation findings, the blade geometry can either obstruct or facilitate dendritic growth, which in turn drives the morphological evolution of slivers.

In the following, a detailed review of sliver defects will be conducted.

3 Review and discussion

3.1 Morphology and structure

According to the morphological features, Xu et al.[63] classified the sliver defects into three groups as follows: (1) a segment of dendrite arm that has developed into a subgrain; (2) an elongated misoriented dendrite; and (3) a developed grain including a cluster of misaligned dendrites that originated from a misoriented dendrite [Figs. 1(a–c)]. Zhang et al.[77] on the other hand, categorized these defects through a different classification: fixed-width, gradually increasing width, and gradually disappearing. Both categories are related to the morphology and evolution of dendrites.

Zhang et al.[77] demonstrated that the difference in sliver morphology cannot be ascribed to competitive dendritic growth, since the misorientation angle between the slivers and the matrix maintains consistently low. They concluded that the geometry of the casting can either hinder or promote dendritic growth, which subsequently influences the morphological development of slivers. However, some studies have attributed the sliver morphology to competitive growth. For example, Huang et al.[68] revealed that significant misorientation in the cross section promotes rapid propagation of slivers along the casting surface and into the interior. Such variation in dendrite branching can be ascribed to the interaction of the solute field from adjacent dendrites within the interdendritic region. Furthermore, the competitive growth behavior between adjacent dendrites has been closely linked to the local solute distribution in these regions. The Peclet number for solute diffusion, denoted as P_c, which is related to the driving force of solute diffusion at the tip of the dendrite, was calculated using Eq. (1)[78, 79]:

$$P_c = \frac{VR}{2D} = \frac{R}{\delta_c} \tag{1}$$

where V represents the withdrawal rate, R denotes the radius of the dendrite tip, D signifies the diffusion coefficient, and δ_c refers to the solute field range. Solute field range δ_c is utilized to characterize the thickness of the solute diffusion layer ahead of the dendrite tip during directional solidification. The value of δ_c is primarily influenced by withdrawal rate V and diffusion coefficient D, in accordance with Eq. (1), and is expressed as follows:

$$\delta_c = \frac{2D}{V} \tag{2}$$

If the distance between adjacent dendrite tips diminishes to the extent that the two solute fields intersect, solute interaction takes place and the growth of dendrites halts; that is, the more pronounced the solute interaction, the less significant the branching effect[79, 80]. In the slivers illustrated in Figs. 2(a) and (c), there is no extension of sliver on the casting surface. In this case, there is a low misorientation between the secondary arms of sliver and matrix. This sliver do not protrude on the casting surface and only develop within the casting gradually.

According to Eq. (2), a solute field range δ_c of around 60 μm was estimated ahead of the dendrite tip in most of Huang's

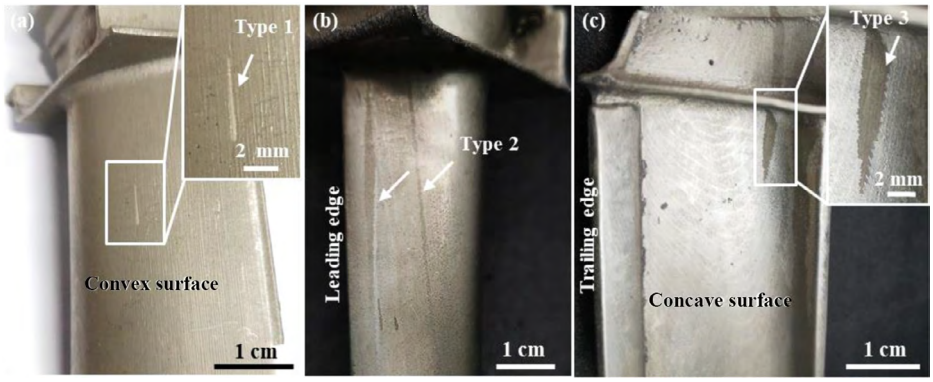

Fig. 1: A segment of dendrite arm that has developed into a sliver defect on the blade convex surface (a), elongated misoriented dendrite near the blade leading edge (b), and a developed grain including a cluster of misaligned dendrites originated from a misoriented dendrite on the blade concave surface (c)[63]

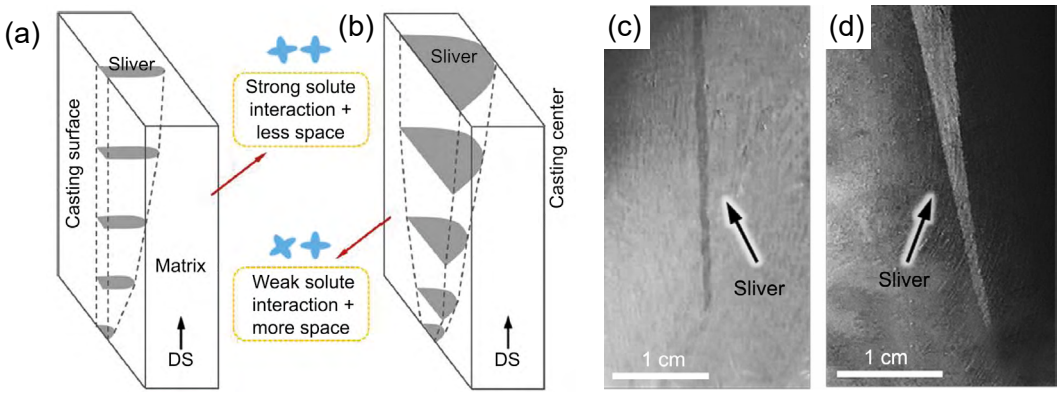

Fig. 2: Schematic (a) and macrostructural (c) illustration of a sliver with a constant width on the surface and gradually extending into the casting (low misorientaion, smaller than 9°, between the sliver and matrix); schematic (b) and macrostructural (d) illustration of a sliver with increasing width on the surface and extending into the casting (large misorientaion, 9.8°, between the sliver and matrix)[68]

experiments[68]. They reported that if a significant misorientation (9.8°) exists between the sliver and the matrix in the cross-section of a casting, the distance between the secondary dendrite tips of the sliver and the matrix will increase to approximately 126 μm, thereby leading to a diminished solute interaction. Moreover, considerable misorientation between the secondary arms also affords greater spaces for dendrite branching. Consequently, the dendrite branching at the sliver/matrix interface is enhanced. The width of this sliver on the casting surface progressively increases, and the dendrites rapidly extend into the casting throughout the directional solidification. Schematic and macrostructural illustration of this branched sliver can be seen in Figs. 2(b) and (d), respectively.

As mentioned above, the relationship between sliver morphology and competitive growth can be expressed as follows: If the solute field of the matrix dendrite prevails over the sliver dendrite, the sliver can be overgrown by the matrix and it does not extend throughout the casting [Fig. 1(a)]. In case of strong interaction between the solute field of sliver and matrix, the sliver is able to extend along the solidification direction without a significant branching [Fig. 1(b)]. Finally, when the sliver's solute field becomes stronger than the matrix, it overgrows the surrounding dendrites and forms a large, branched grain consisted of many dendrites [Figs. 1(c) and 2(b, d)]. It should be noted that the misorientation of the sliver and the matrix relative to the solidification direction has a significant effect on the solute field and consequently the morphology evolution of the sliver. This effect was also discussed in the previous paragraph. The misorientation of the slivers will be discussed in detail in Section 3.2.

Sometimes, slivers may be confused with other grain defects such as freckles. The distinctive feature of slivers is their low misorientation angle with respect to the matrix dendrites[68, 74]. Meanwhile, freckles appear in the form of randomly oriented equiaxed grains (severely misoriented)[53, 65, 81-83]. Therefore, by using texture analysis techniques such as electron backscattered diffraction (EBSD), slivers and freckles can be easily distinguished. However, due to the limited access to advanced structural analysis equipment in many cases, it is necessary to examine the macrostructural and microstructural differences between slivers and freckles. In Fig. 3(a), the macrostructure of a single crystal casting is illustrated. There are two slivers, Sliver 1 and Sliver 2, present in the extended zone between the grain selector and the casting. The starting point of the slivers is connected to a freckle defect. Therefore, freckles can lead to the initiation of the misoriented sliver grains. As illustrated in the high-magnification image in Fig. 3(a), the slivers manifest as deviated dendrites, whereas

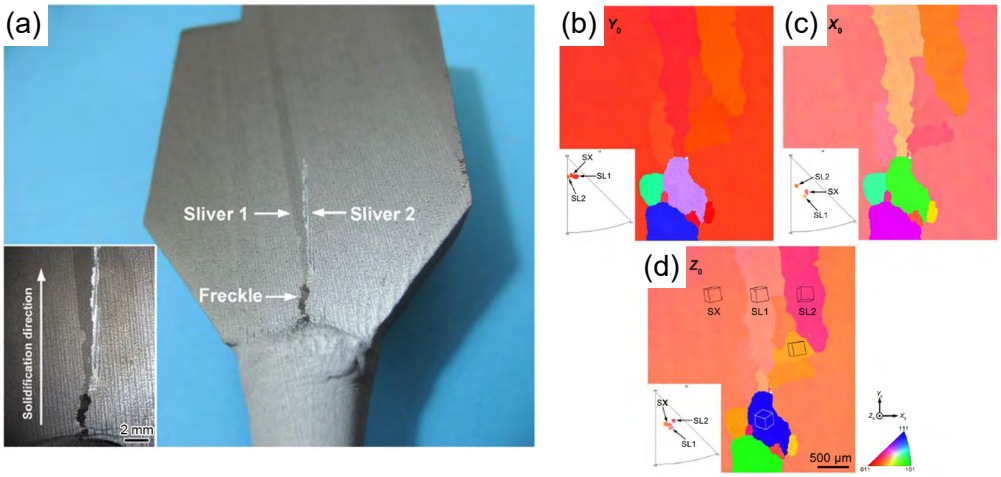

Fig. 3: Macro-etched morphology of a single crystal superalloy casting (a), and orientation map and corresponding IPFs for the casting in Y_0 (b), X_0 (c), Z_0 (d) directions[65]

freckles appear as dark regions[65]. Some optical micrographs of freckle[16] and sliver[65, 69] defects in single crystal superalloys are shown in Fig. 4. As can be seen, slivers are individual and keep their dendritic configuration, while freckles consist of fragments of broken dendrites that are observed as a chain along the solidification direction (gravity). Another way to distinguish freckles from slivers is to use energy dispersive X-ray spectroscopy (EDS). Freckles are usually rich in low melting point compounds. As a result, their chemical composition is similar to the interdendritic regions and eutectic islands[44, 81]. However, there is no report of difference between the slivers and matrix alloy composition.

3.2 Misorientation

In the literature, sliver defect has been typically mentioned as a low-angle misoriented grain[66, 68]. Huo et al.[84] reported

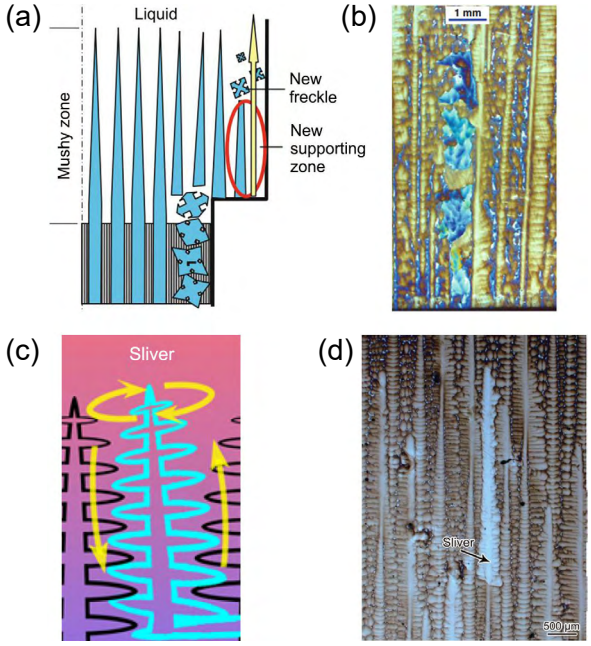

Fig. 4: Schematic illustration and optical image of a freckle chain (a, b)[16], and a sliver defect (c, d)[65, 69] in a single crystal superalloy

that sliver defects introduce longitudinal low-angle grain boundaries (LABs) during solidification. Figures 3(b–d) depict the crystallographic texture within the magnified figure on the lower left corner of Fig. 3(a). Deriving from the inverse pole figure maps (IPFs), different features such as single crystal, Sliver 1, Sliver 2, and freckle grains have been colored based on their crystal orientations with respect to the directions of Y_0 [Fig. 3(b)], X_0 [Fig. 3(c)], and Z_0 [Fig. 3(d)]. The results show that the freckles have random orientations that differ greatly from the orientation of the single crystal. The primary crystallographic orientation of Sliver 1 closely aligns with that of the single crystal along the Y_0 growth direction (solidification direction), but significant misorientation is observed in the X_0 and Z_0 transverse directions (perpendicular to the solidification direction). In other words, Sliver 1 turns on its axis in the solidification direction more than it tilts relative to the single crystal. Figures 3(b–d) illustrate that Sliver 2 has a greater inclination and rotation angle compared to the single crystal, as depicted in the IPFs. Misorientation angle range of the slivers and freckles in Fig. 3 were reported 3°–18° and 15°–57°, respectively[65]. To gain a better understanding of the crystal misorientation of slivers, the results of a number of research works are presented in Table 1. According to the resulted data, the misorientation angle of slivers varies from 3° to 18°.

Transmission electron microscopy (TEM) can provide insights into misorientation of grain defects in single crystal

Table 1: Crystal misorientation of slivers in the literature

Sliver misorientation angle	Reference
3°–18°	[65]
3.5°–9.8°	[68]
<10.05°	[66]
<15.5°	[71]
6.5°–13.9°	[74]
3.2°–12°	[63]

superalloys. The results of TEM analysis of the boundary region between sliver and matrix in a single crystal casting is illustrated in Fig. 5[63]. The grain-boundary can be seen inside the white circle region in Fig. 5(a). The selected area electron diffraction (SAED) pattern of the grain-boundary is represented in Fig. 5(b). The result suggests that the grain-boundary exhibits a 5.7° misorientation about the [001] direction. This reveals that the dendrite trunk has undergone rotation during the solidification process, ultimately leading to fragmentation and the formation of a sliver defect[63].

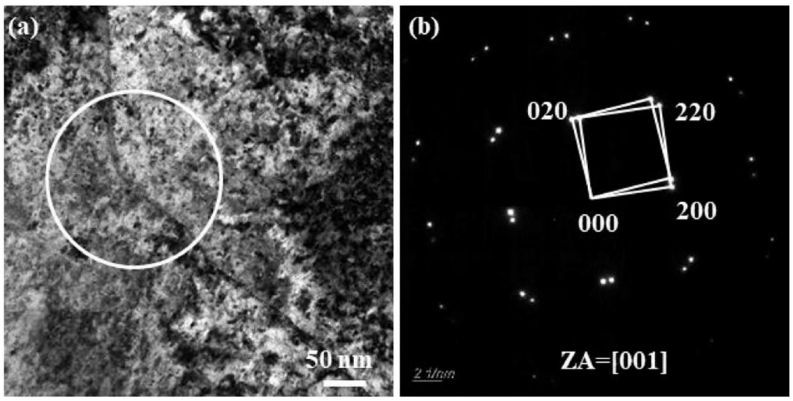

Fig. 5: TEM image displaying the grain boundary (GB) (a) and SAED pattern corresponding to the GB region indicated by the white circle in (a) (b) [63]

3.3 Formation mechanism

Various mechanisms have been proposed for slivers formation. These mechanisms are listed in Table 2. In a previous study on forecasting a process window for investment casting of single crystal superalloys, slivers were descried as stray grains caused by unwanted nucleation in the undercooled melt at the interface of solid/liquid due to unfavorable process conditions[85]. It has also been stated that slivers usually come from defects on the inner surface of ceramic moulds, and the formation of stray grains may be due to heterogeneous nucleation promoted by mould surface defects[17]. Nevertheless, examination of the crystal structure of the slivers in subsequent studies[63, 74] disproved the nucleation hypothesis. Because, most of the sliver grains show little deviation from the matrix, while the nucleated grains are typically randomly oriented[63].

Dendrite fragmentation (detachment/fracture/tearing) as well as dendrite deformation are the most dominant mechanisms for the formation of slivers in single crystal superalloys. Some studies have considered the dendrite fragmentation as a sliver formation mechanism[63, 69, 71]. However it seems that the hypothesis of dendrite deformation is more acceptable in the literature[64-68, 74, 75]. Literature review shows that both hypotheses can be authentic for explanation of the slivers formation. It should be noted that despite the possibility of dendrite fragmentation during the formation of slivers, their deviation from the matrix crystal growth direction is limited[63, 69, 71]. While, in the freckle formation mechanism, the fragmented dendrites are immersed in the melt and form a chain (trail) of stray grains with random crystal orientation[86-88].

Ma et al.[69] examined the origin of dendrite fracture (fragmentation) in a single crystal superalloy casting. Figure 6(a) shows a sliver grain on the surface of a blade casting after macroetching. Through the magnification of the microstructure in Figs. 6(b–d), one can see that a sliver crystal originates from the fracture that occurred during the growth of a certain columnar dendrite. The dendrites at the lower part of the fracture surface exhibit the same orientation as the surrounding dendrites and are a part of the single crystal matrix structure. In the high-magnification view of Fig. 6(d), it can be found that the fracture originating from the sliver grain is filled with a thin film-like structure. This is because the gap formed after the dendrite is filled with the low-melting-point residual liquid between the dendrites. These residual liquids in the final stage of solidification are enriched with positively segregated elements (e.g. Ti, Al, and Ta), therefore, this liquid film finally solidifies into a γ' phase structure, which is significantly different from the matrix structure on both sides of the fracture surface. From the SEM image in Fig. 6(e), it can be confirmed that this continuous fracture zone is rich in γ' phase (eutectic structure) and has been generated directly from the residual liquid.

Xu et al.[63] indicated that dendrite fragmentation is caused by macroscopic and microscopic nonuniform stresses. They also proposed that in the mushy zone during solidification, dendrite fragmentation occurs easily instead of undergoes significant plastic deformation. Therefore, the dendrite fragmentation is a consequence of insufficient dendrite plasticity in the mushy zone. However, most researchers[64-68, 74, 75] consider dendrite deformation as the basic mechanism of sliver defect formation. Aveson et al.[89] utilized synchrotron X-ray imaging to study the in situ dendrite deformation during directional

Table 2: Sliver formation mechanisms

Sliver formation mechanism	Reference
Heterogeneous nucleation (on the mould wall, oxide layer, etc.)	[17], [85]
Dendrite-fragmentation/detachment/fracture/tearing	[63], [69], [71]
Dendrite deformation	[64–68], [74], [75]

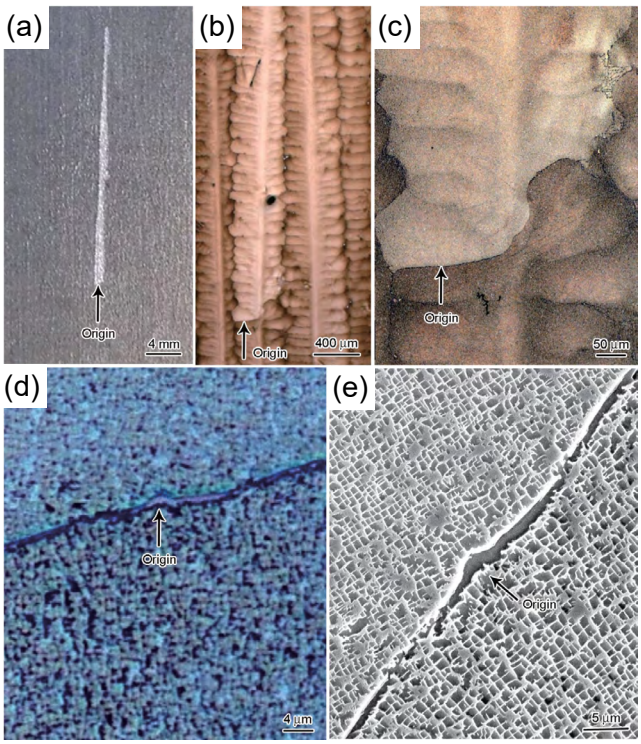

Fig. 6: A sliver defect originated from dendrite fracture (fragmentation): (a) macrostructure; (b–d) optical micrographs; and (e) SEM micrograph illustrating the microstructure of the sliver origin[69]

solidification of a Ni-based superalloy. They observed that dendrite deformation could be accomplished through various mechanisms. Permanent and transient deformations, as well as local and cumulative deformations, were observed. Although some deformations could be directly attributed to the gravitational loading of the dendrites, other modes of deformation appeared to result from other transient stresses. Figure 7(a) illustrates the radiographs of the growing dendrites. In the first radiograph, four dendrites are labeled. In the starting frame, the dendrites are aligned in a parallel manner. However, in the following pictures, Dendrite 3 deviates from the other dendrites. The bending happens erratically and is concentrated at a point around one-third of the image's height[89]. According to previous experimental and numerical studies, dendrite deformation occurs in three dimensions and involves mechanisms such as bending and torsion[63, 66, 89]. A schematic representation of the dendrite deformation modes can be seen in Fig. 7(b).

3.4 Factors contributing to sliver initiation

Dendrite misorientation and sliver defect formation are widely attributed to localized stresses imposed on dendrites during directional solidification[63-69, 71, 74, 75, 90]. The non-uniform stresses can eventually lead to fracture (fragmentation)[63, 69, 71] or plastic deformation of dendrites[64-68, 74, 75]. Various factors can influence

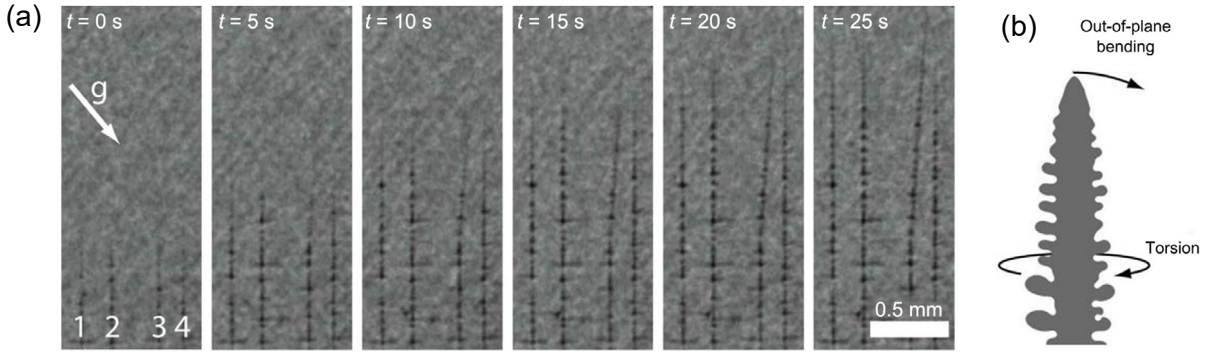

Fig. 7: Chronological order of the radiographs illustrating the correlation between dendrite deformation and the growth kinetics of dendrites (a), and schematic representation of a primary dendrite arm labeled with dendrite deformation modes (bending and torsion) (b)[89]

the intensification of the stress non-uniformity on dendrites and as a result, deviation in dendrite growth direction and the presence of the sliver grain defects in the casting. In the following subsections, the most important factors contributing to the formation of slivers in single crystal superalloys will be described.

3.4.1 Inclusions

Inclusions have a significant impact on the fatigue life of both cast and wrought alloys when subjected to cyclic loading conditions within the elastic range[91]. The different types, origins, and formation mechanisms of inclusions in Ni-based superalloys are a result of the intricate preparation process and high degree of alloying[92]. These impurities primarily originate from raw materials, refractory components used during melting or casting, and in-situ nucleation during the solidification process[93]. According to their sources, inclusions in Ni-based superalloys can be classified into endogenous and exogenous inclusions. Endogenous inclusions are formed when impurity elements (e.g. oxygen, nitrogen, sulfur) in the melt react with active elements and form through precipitation, collision, and aggregation processes during solidification. Exogenous inclusions are caused by the peeling of refractory material in the bottom of the mould or the peeling of a crucible[94]. There is not a consensus about the role of inclusions in the sliver formation. While, according to Aveson's research[74], oxides play no role in the sliver formation. Some studies[63, 69, 71, 95] have considered oxide inclusions as a possible origin of sliver defects. Previous studies[63, 69, 71] have indicated that in cases where oxide inclusions are implicated in sliver formation, dendrite fracture (or fragmentation/tearing) is generally considered the dominant mechanism of sliver generation. In

addition, occurrence of inclusions during solidification can lead to local stress concentration[96], which may result in a brittle dendrite fracture rather than plastic deformation.

Figure 8(a) shows a sliver grain on the surface of a single crystal blade. There are multiple Pt pinning wires on the blade surface forming hulls, but the sliver crystals have not been generated at these locations. They originated from a smooth surface. It should be noted that pinning wires are used during mould preparation and investment casting of the blades for reliable manufacture of the cooling channels. Their primary function is to maintain the position of the ceramic cores during mould preparation and casting. After metallography of the specimens, large groups of oxide inclusions are found at the origin of the sliver defects [Figs. 8(b, c)]. It is believed that these inclusions greatly weaken the strength of the dendrites and cause the dendrites to tear during solidification shrinkage[69].

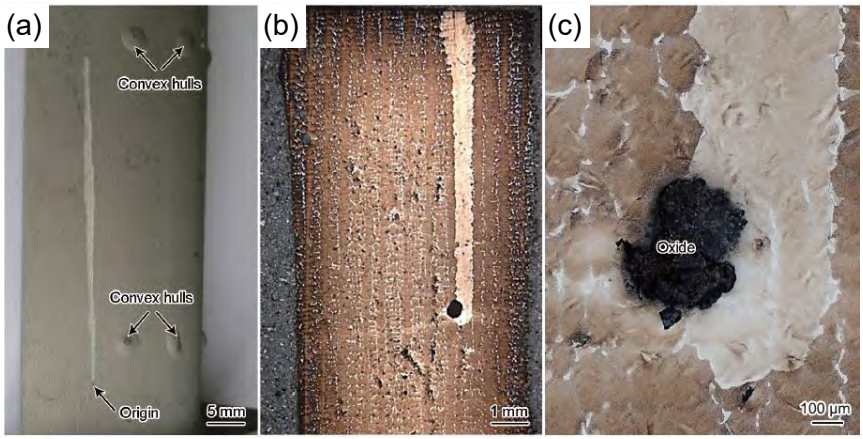

Fig. 8: Macrograph of a sliver defect at a single crystal blade surface (a), and optical micrographs of the sliver showing an oxide incusion as the sliver origin (b, c)[69]

Xu et al.[63] and Xia et al.[71] reported the simultaneous presence of inclusions and pores (voids) as a potential origin of sliver initiation. In Fig. 9(a), a longitudinal sliver with oxide inclusions and porosities is visible on the surface of the casting. Figure 9(b) shows the SEM image of a common pore. It can be seen that the microstructure is divided by the pore and then partially joined back together. A complex microstructure characterized by coarse γ' precipitates, oxide inclusions, and microcracks can be observed in the rejoined area, as illustrated in Fig. 9(c). EDS map reveals the presence of alumina oxides, which could originate from mould surface or oxide films formed during casting [Fig. 9(d)]. Microstructural tearing is observed in the separation area close to the pore. In Fig. 9(e), the presence of a crack with a rough interface indicates that it formed after solidification due to thermal stresses generated during the cooling process. Additionally, the inner surface of the pore is covered with numerous spherical particles, which are believed to be low-melting-point phases formed during the final stage of solidification. This morphology indicates that the pores formed during the solidification process [Fig. 9(f)]. These observations indicate that dendrites may experience intricate stress during solidification in the presence of inclusions and pores, potentially leading to dendrite fragmentation due to the induced stress concentrations[63].

The pore morphologies at the starting point of the sliver defects formed during solidification of a RenéN5 single crystal superalloy are shown in Figs. 10(a1–c1). From the composition and orientation analysis result of Figs. 10(a1–a3), it can be seen that the voids (pores) mainly consist of O and Al, which are the primary elements of oxide inclusions in nickel-based superalloys. An additional EPMA examination has been conducted on the remaining two sliver pores. It is observed in Figs. 10(b2, c2) that, except for Al and O, the defects also exhibit unexpected enrichment of other two elements, C and Si. The RenéN5 superalloy does not contain any Si element, and the C element present is only around 0.05wt.%, which is not sufficient to cause such significant enrichment. These elements are not sourced from the master alloy. In contrast, the primary components of the shell materials in this study are Al, O, Si, and C elements. The composition distribution in the pores shown in Figs. 10(b2, c2) is also consistent with these four elements. In addition, based on the EDS findings in Figs. 10(b3, c3), the pores and inclusions show significant enrichment of Si and C elements, while their presence in the surface area is minimal. Consequently, the pores and inclusions that result in sliver defects, are directly associated with the mould shells[71].

Therefore, to avoid the formation of inclusions, as a factor contributing to sliver formation during directional solidification of superalloys, it is necessary to take the following considerations: (1) establishment of high vacuum during casting to minimize gas content within the melt; (2) maintain stability of the refractory materials (crucible and mould).

3.4.2 Solidification pores (voids)

During the solidification process, porosity formation is an inevitable phenomenon, as its compensation through interdendritic liquid flow is difficult[97]. This can significantly affect the thermal and mechanical properties of the castings[98-100]. In addition, some studies have considered the pores (voids) as a factor contributing to the sliver initiation[63, 71]. In Figs. 9 and 10, it could be seen that the pores and inclusions might be

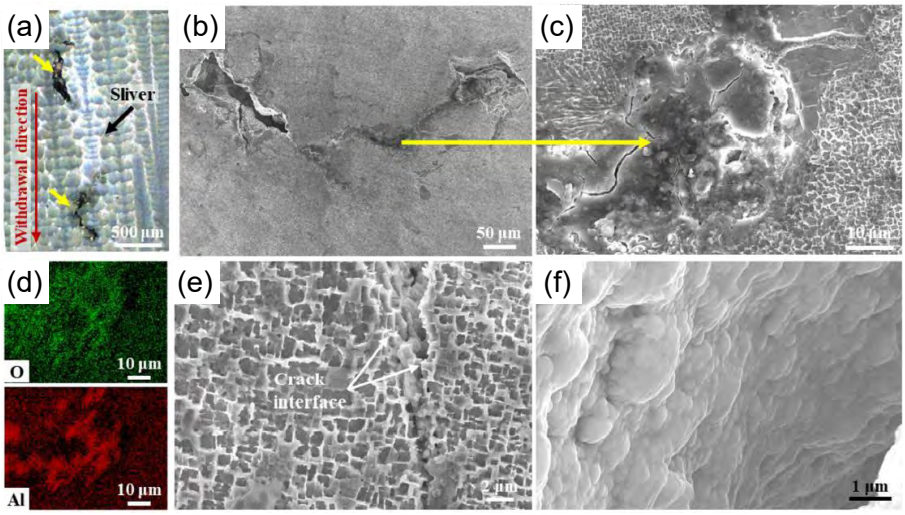

Fig. 9: Optical micrograph of a sliver defect (a), SEM micrograph of a solidification pore (void) (b), higher magnification image of the rejoined area in (b) (c), EDS results revealing O and Al distribution for the area shown in (c) (d), interface of the crack displaying microscopic tearing (e); and the inner surface of a pore (f)[63]

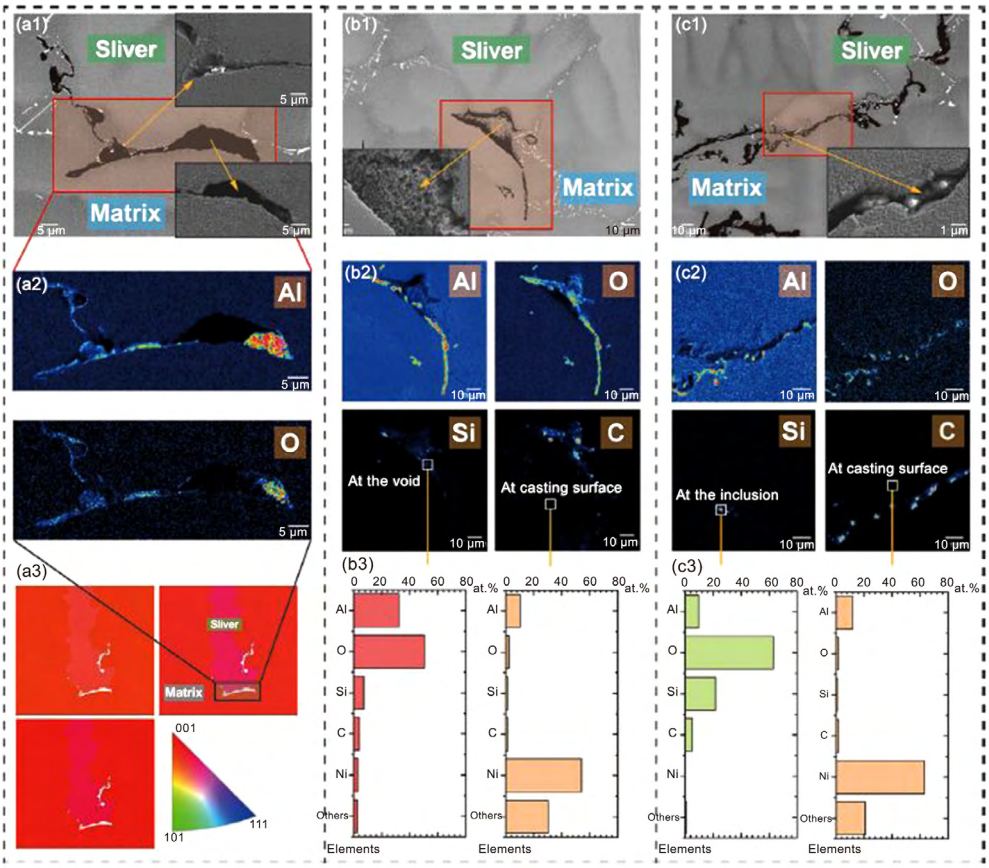

Fig. 10: Backscattering and secondary SEM images of the pores (voids) at starting point of sliver defects (a1–c1), EMPA results on pores (a2–c2), EBSD map of sliver defects (a3), EDS results for the marked area (b3, c3) [71]

interconnected to each other. Xia et al.[71] classified the sliver defects based on the presence of voids at the initial position of the defect. As reported in their study, out of eight sliver defects identified in the castings, two were found to originate from voids located in the initial region. The authors noted that most slivers exhibited misorientation angles of less than 8°, with the exception of the two slivers initiated at voids, which showed significantly higher orientation deviations of 15.5° and 10.5°, respectively. Therefore, it can be concluded that the presence of voids during solidification can facilitate the dendrite fragmentation and lead to the formation of slivers with a higher deviation angle. This can be connected to the high local stress concentration in the voids (pores) region[101]. At the same time, the presence of inclusions nearby the voids can intensify the stress concentration. Figure 11 shows the macro and micro-graphs of the sliver defects in a single crystal superalloy from Ref. [71]. Figures 11(d, e) demonstrate the OM and SEM images of the sliver initiation area. According to the irregular

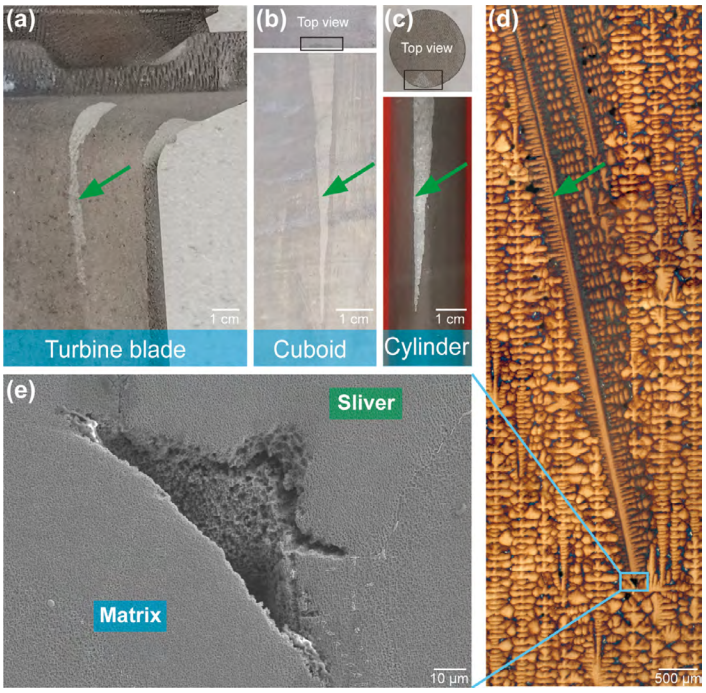

Fig. 11: Morphology of sliver defects on three different single crystal components: (a) blades; (b) cuboid castings; (c) cylindrical castings; (d) optical micrograph of a sliver defect; and (e) SEM image of a pore (void) at the initial region of sliver[71]

morphology of the void in Fig. 11(e), it can be considered as a solidification (shrinkage) micro-pore[98].

Plancher et al.[102] studied the mechanisms of pores formation during solidification of a Ni-based superalloy utilizing 4D synchrotron microtomography. They identified two mechanisms resulting in the shrinkage pores. Mechanism A is linked to the merging of secondary dendrite arms at a high temperature in the initial solidification stage. While, Mechanism B is connected to a lack of liquid feeding in the interdendritic area at lower temperatures towards the end of solidification. They also characterized the kinetics of individual pore growth, and proposed that Mechanism A exhibits faster kinetics than Mechanism B. In addition, a variation of cooling rate does not influence the nucleation kinetics of pores formed through Mechanism B. However, it appears to impact the nucleation rate of the fine pores produced by Mechanism A. Consequently, one can say that the formation of shrinkage pores during solidification is inevitable. However, by optimizing the solidification parameters, the pores content may be reduced to some extent. The formation of porosity is largely influenced by three factors: thermal gradient (G), withdrawal rate (R) of the mould, and the alloy shrinkage factor[97, 98]. Thermal gradient and withdrawal rate are the most critical solidification parameters that affect the final structure of the directionally solidified components. By optimizing these parameters, it is possible to achieve the finest dendritic microstructure with the minimum amount of solidification defects[103-108]. It is important to point out that, during directional solidification process, a high thermal gradient is always desirable. By increasing the thermal gradient, the withdrawal rate can be increased without creating critical solidification defects such as freckles[60, 106, 109]. In general, by increasing G and R, the solidification (cooling) rate will be enhanced and a finer dendritic structure will be obtained in the casting[9]. The resulting fine dendritic structure can limit the interdendritic space and eventually a finer distribution of pores will appear in the structure[20, 98]. It seems that no study has been conducted on the alloy shrinkage factor as the third effective parameter in the formation of shrinkage pores, with an emphasis on superalloys.

3.4.3 Geometrically complex areas

Single crystal components generally possess complex three-dimensional geometries such as curved surfaces (convex and concave surfaces), rejoined platforms, cooling holes, grain selectors, and extended sections. These geometrical complexities can lead to a local stress concentration during solidification. Therefore, dendrite deformation and dendrite fragmentation are more likely to occur in these areas[63, 66, 67, 75, 110].

Huo et al.[67] studied the sliver formation in the extended cross-section platforms during solidification of a single crystal superalloy. To prepare the single crystal castings, a configuration with five rejoined platforms was utilized [Fig. 12(a)]. They also used ProCAST software for finite element analysis to model the casting process, showing the thermal profile and evaluating the transient stresses occurred during directional solidification. Figures 12(b–f) display the effective stresses at various heights as the liquidus (white line, 1,399 °C) and solidus isotherm (black line, 1,342 °C) move. In Fig. 12(b), the platform does not experience any stress at 2,041 s because the metal is still in a liquid state. Twenty seconds later, a slight stress of 4 MPa was applied to the section extension area, as shown in Fig. 12(c). As the solidification front advances, the effective stresses at this location steadily rise, with the maximum effective stress exceeding 30 MPa, as depicted in Figs. 12(d, e).

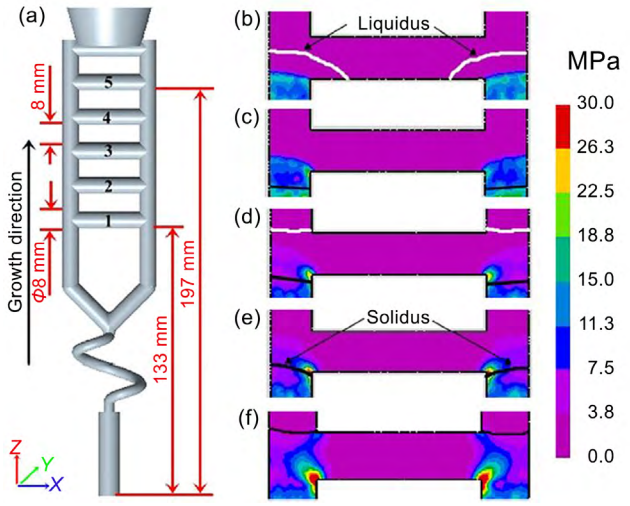

Fig. 12: Schematic of the sample with five rejoined platforms (a), and variation in total effective stress during solidification process as the liquidus (white line) and solidus (black line) move forward in a platform: (b) *t*=2,041 s; (c) *t*=2,061 s; (d) *t*=2,081 s; (e) *t*=2,121 s; and (f) after solidification[67]

Interestingly, there is no visible stress at the center of the platform until the solidus line shifts to the location shown in Fig. 12(f). As the solidification process progressed, stress could arise in the central region; however, by that time, the dendritic growth had already been completed. Consequently, this late-occurring stress did not influence dendrite growth itself, although dendrite deformation was still observed to occur in the mushy zone. The development of stress field facilitated the generation of bending moment and torque in the section extension region. As a result, stress concentrations in the geometrically complex areas, including rejoined platforms, can lead to sliver formation in these regions.

Moreover, Fig. 13 shows how the thermal field of the platform changes as the solid-liquid interface advances. Clearly, when the solid-liquid interface reached the platform region, it transitioned from being flat to having a curved shape. The interface slanted towards the inside and created a tilt at the section extension area, as depicted in Figs. 13(a) and (b). In simpler terms, it was observed that heat extraction in this region occurred predominantly in the lateral direction. This

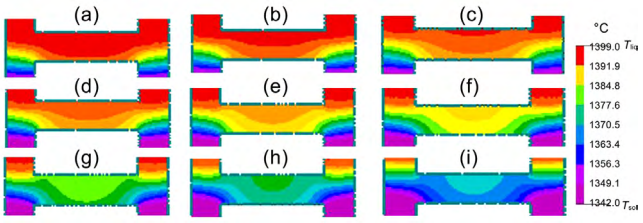

Fig. 13: Evolution of thermal field and solid-liquid interface shape in the platform during solidification of a single crystal superalloy: (a) *t*=2,061 s; (b) *t*=2,071 s; (c) *t*=2,081 s; (d) *t*=2,091 s; (e) *t*=2,111 s; (f) *t*=2,121 s; (g) *t*=2,151 s; (h) *t*=2,181 s; and (i) *t*=2,191 s[67]

condition favored the easy development of secondary dendrite arms. Afterwards, the solid-liquid interface was less inclined, as depicted in Figs. 13(c–e), and ultimately became more flat, as can be seen in Figs. 13(f–i). Moreover, the thermal distribution in the section extension area was inhomogeneous, which could lead to stress concentration. This is attributed to the difference in thermal contraction coefficients between the mould and the molten metal, resulting in inherent contraction stresses during solidification and cooling[67].

Xu et al.[63], in their work, studied the effect of airfoil geometry on sliver formation. The cross section along the blade vertical axis featured a consistent twist from the airfoil tip to the bottom. In the airfoil section of the blade depicted in Fig. 1, the typical cross-sections (S1 and S2) are arranged along the vertical axis of the blade (*Z*) from top to bottom [Fig. 14(a)]. It can be observed that the twist caused the leading edge contour to shift towards the side of the convex surface, with a minimal change in the position of the trailing edge [Fig. 14(b)]. During directional solidification, the preferred grain is typically started from the tip of the blade, with the withdrawal direction aligned parallel to the vertical axis of the blade. It is unavoidable for dendrites to contact with the mould wall during growth due to the constraints imposed by the airfoil geometry. In a typical longitudinal cross-section (S3) parallel to the vertical axis, an inclination was observed on the airfoil surface [Fig. 14(c)]. When the primary dendrites grow in alignment with the vertical axis, a converging interface will develop on the convex surface, and a diverging interface will form on the concave surface. These converging and diverging angles are represented by α and β, respectively [Fig. 14(c)].

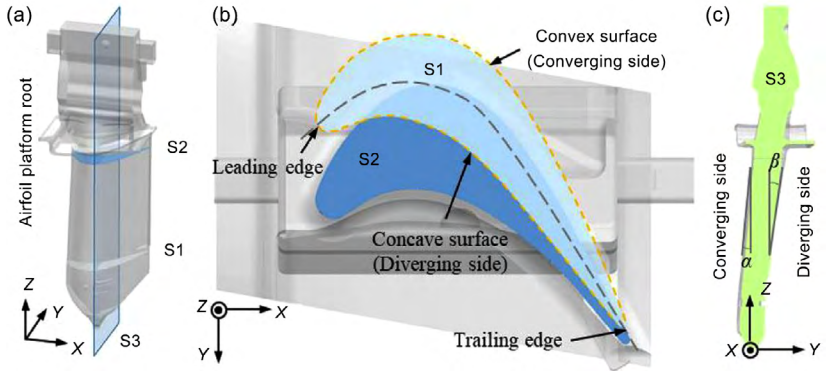

Fig. 14: Schematic of a common blade (a), cross-sections (S1 and S2) (b), and longitudinal section (S3) (c) of a turbine blade[63]

This model suggests that the formation of sliver is more likely on the convex surface due to the vulnerability of dendrite deformation at the converging interface. Formation of the sliver defects near the leading edge on the convex surface, as seen in Fig. 1(a), matched the prediction due to dendrite deformation vulnerability at the converging interface. In this region, the local dendrite growth direction converged slightly towards the mould wall. Additionally, the dendrite deflection and sliver formation can be influenced by factors such as grain orientation, solid-liquid interface morphology, and dendrite arm size. Therefore, the sliver defects could occur at the concave surface, as depicted in Fig. 1(c), when the selected grain orientation significantly deviates to this surface (the interface becomes converging).

Yang et al.[75] studied the sliver formation in C-shaped grain selectors during investment casting of a single crystal superalloy. They announced that the origin of sliver depends upon tensile stress during solidification, relying on the constraints of dendrite boundaries. They also suggested that the joint sections of the starter block, i.e., selector and selector-casting joint of C-shaped selector sections, are stress-sensitive areas where sliver can form readily. As shown in Fig. 15, there is a sliver in the necking channel between the C-shaped selector and the casting. One can deduce that when the solid-phase isotherm passes through the necking channel, stress gathers in the channel, and when the stress value is more than the yield strength of superalloy near the solidus, dendrite deflection occurs, resulting in the occurrence of slivers. Therefore, grain selectors can be considered as potential sites for the initiation of sliver defects.

3.4.4 Mould wall

Detailed examination by Huang et al.[64, 68] revealed that slivers could originate from the localized deformation of one to two dendrites near the mould wall at the diverging boundary, with thermal contraction force being a key factor in its formation. Other studies also have mentioned the mould wall as a facilitating factor for sliver formation. The primary cause of this outcome has been considered the varying thermal contraction coefficient between the mould material and the liquid metal[69, 71, 74]. The schematic illustration suggested by Ref. [64] (Fig. 16) shows how the sliver defect is formed due to thermal contraction. In Fig. 16(a), it can be observed that three tertiary dendrite arms (I, II, and III) are developing from a secondary dendrite within the mushy zone. This occurs when a primary dendrite deviates from the direction of directional solidification process due to a change in casting geometry, and dendrite bridging forms (indicated by the red circles). In the meantime, thermal contraction causes downward (F_z) and inward (F_x) forces on the solidified dendrites in the mushy zone due to the geometric restrictions of the ceramic mould, as shown in Fig. 16(b). These forces can be resolved into components along (F_c and F_d) and perpendicular (F_a and F_b) to the dendrite axis, respectively. One can see that the forces

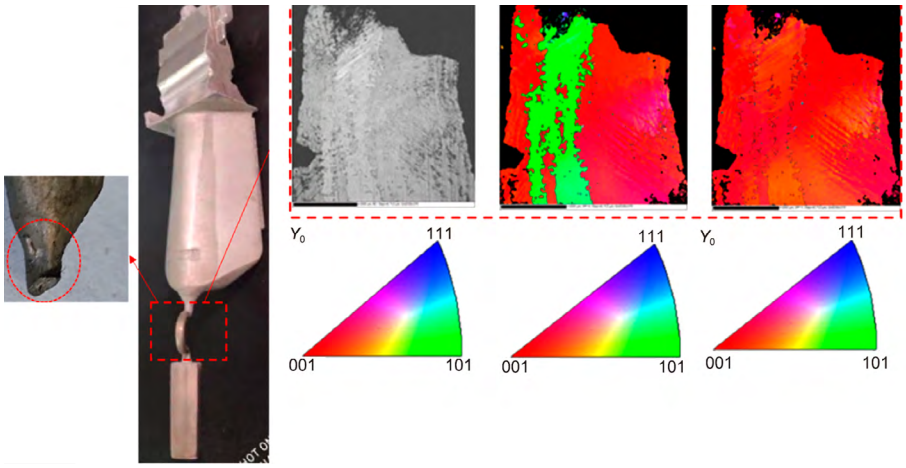

Fig. 15: Illustration of longitudinal dendrites of sliver in the necking channel of a casting solidified by C-shaped grain selector[75]

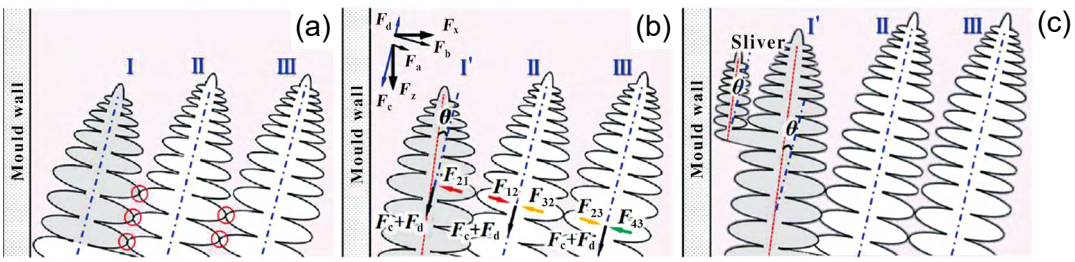

Fig. 16: Schematic representation of sliver defect formation mechanism: (a) evolution of new dendrite close to the mould wall and occurrence of dendrite bridging; (b) dendrite deformation caused by unbalanced force resulting from thermal contraction; (c) sliver defect arisen from the deformed dendrite growth[64]

F_c+F_d will cause the dendrites to move downwards relative to the dendrite axis, while the forces F_a+F_b will be transmitted between the connected dendrites. Dendrite II is under the influence of forces F_{12} and F_{32} from Dendrites I and III, but it will remain undeformed due to the balance of forces. Likewise, Dendrite III experiences balanced forces F_{23} and F_{43} from Dendrites II and IV (not shown in Fig. 16), with no deformation occurring within it. However, the lower section of Dendrite I close to the mould wall is prone to undergoing mechanical deformation; because the force F_{21} (F_{21}=F_a+F_b) exerted by neighboring Dendrite II is unbalanced, resulting in misorientation (θ) between Dendrites I' and II (or III). There is no connection (bridging) between the secondary dendrite arms on the top section. Therefore, it is anticipated that there will be no deformation in this region. Figure 16(c) illustrates that the lateral growth of Dendrite I' inherits the misorientation (θ), but without strain. The growth of the deformed Dendrite I' persists, branching out at the diverging boundary until a sliver defect is ultimately formed. It can be believed that only the dendrites that have well-established branches (increased bridging leading to stress transmission) at the diverging boundary may develop into sliver. On the other hand, a more aligned [001] dendrite axis with reduced branching will have a lower possibility of creating slivers. Additionally, the reduction of thermal contraction force is also a crucial factor, achieved through modifying mould materials and processing[64].

Xia et al.[71] found that during the solidification process, if a dendrite comes across a protuberance on the shell (mould) surface, it will keep growing and eventually wrap the protuberance (Fig. 17). Hence, a vulnerable region will be created by a dendrite, which is easier to fracture when exposes to stress compared to other areas. During solidification process, the alloy has a greater amount of shrinkage compared to the shell material. Due to the varying shrinkage rates of the dendrite and shell protuberance, a high stress region forms at the bulge of the mould shell, leading to increased susceptibility of dendrite fracture and greater orientation deviation. Accordingly, it can be concluded that the surface quality of the wax pattern as well as the ceramic shell is of great importance as the presence of any surface protuberance can lead to the appearance of grain defects, including slivers.

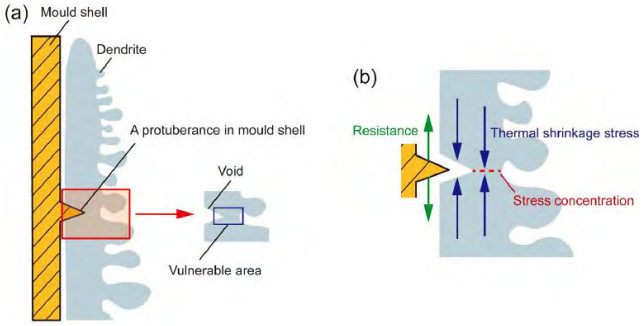

Fig. 17: Schematic of sliver formation mechanism induced by mould shell protuberance: (a) morphology of the shell protuberance wrapped by a dendrite; (b) stress condition at the shell protuberance and dendrite[71]

3.4.5 Freckles

Freckles are a group of well-known detrimental grain defects leading to a high-rate rejection of directionally solidified components (both columnar grain and single crystal parts)[111-113]. Meanwhile, slivers, as a group of low-to-medium angle grain defects have been noticed in recent years, and their formation mechanisms in single crystal superalloys have been studied.

Han et al.[65] revealed that in the extended area of single crystal castings, freckles can lead to the generation of sliver defects. The evolution of freckles into sliver defects is shown in Fig. 3. In addition, the evolution of a freckle defect into a sliver grain is schematically depicted in Fig. 18. During directional solidification, thermal stresses can develop within freckle channels due to solidification shrinkage of the solute-enriched region. The dendrite deflection and rotation arisen by this thermal contraction force on the bottom of the dendrite arm near the freckle channel, as well as further development of the deformed dendrite, can lead to the formation of a sliver grain. A potential evolutionary link between freckles and sliver defects has not been previously reported in the literature. Therefore, further research is needed to gain a deeper insight into this mechanism.

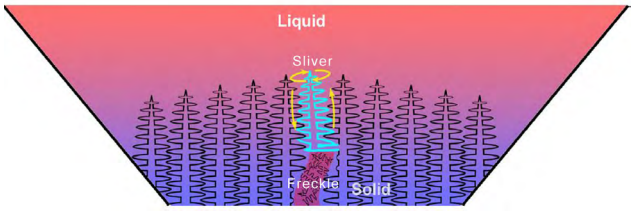

Fig. 18: Schematic illustration of the evolution of freckle defects into sliver grains[65]

3.5 Effect of slivers on mechanical properties

In general, the presence of any grain defects that decrease the integrity of a single crystal casting can affect its mechanical properties[114-121]. As mentioned in the previous sections, slivers are a group of grain defects with low-to-medium angle misorientations that can form through two primary mechanisms: dendrite deformation and dendrite fragmentation. Huo et al.[84] reported that a type of longitudinal low-angle boundaries (LABs) is introduced by the sliver defects. Effects of grain misorientation on the mechanical properties of single crystal superalloys have been investigated by many researchers. Li et al.[118] investigated the effect of misorientation on the fatigue life of a DD5 single crystal superalloy. They carried out the fatigue tests of the samples with different misorientation angles in the range of 3.85°–12.1° at 980 °C. The results confirmed that with an increase in misorientation angle, the fatigue life decreases. Furthermore, the orientation sensitivity of fatigue life is affected by stress level, and it is more sensitive to misorientation at a low stress. Huang et al.[122] concluded that when the misorientation angle is larger than 10°, μ phases can precipitate at grain boundaries and consequently, deterioration of the mechanical properties is expectable. In addition, Li et al.[119] reported that low-angle boundaries (LABs)

clearly impact the creep rupture life of a single crystal superalloy at elevated temperatures. This is attributed to the strong role of diffusion in the creep deformation at high temperatures, so that a great number of microcavities can be seen in the creep rupture specimens. Growth and inter-linkage of these intergranular microcavities lead to crack propagation and finally fracture of the specimens[123].

According to the above-mentioned considerations, it can be expected that due to the inherent misorientation of the slivers, the presence of these defects will lead to a decline in mechanical properties. However, Yu et al.[76] has conducted the only recent research on the mechanical properties of the castings containing sliver defects. They conducted a detailed study on the sliver defect in the second-generation Ni-based single crystal superalloy CMSX-4, focusing on its influence on creep performance at 980 °C/250 MPa. For this purpose, they prepared single crystal specimens containing sliver defects in a vacuum directional solidification furnace using the spiral crystal selection technique. To minimize other factors' interference, specimens with and without sliver defects were cut from the same specimen, as shown in Fig. 19(b). The macroscopic morphology of the sliver defect is illustrated in the arrow part of Fig. 19(c). The grain orientation test results in the gauge section of the stress-rupture specimens are shown in Fig. 20. It is evident that the gauge section of the specimen without a sliver defect consists of a [001]-oriented single crystal. In contrast, the gauge section of the specimen containing a sliver defect is penetrated by a misoriented sliver crystal. The creep-rupture (stress-rupture) tests were conducted under experimental conditions of 980 °C/250 MPa, and the creep-rupture properties of the specimens without sliver and with sliver after heat treatment are listed in Table 3. Sample 1, without sliver in the gauge section, shows a creep rupture life of 143.35 h, an elongation of 16.00%, and a reduction in cross-sectional area of 9.98%. Sample 2, with sliver in the gauge section, exhibits a creep rupture life of 105.55 h, an elongation of 5.20%, and a reduction in cross-sectional area of 5.88%. The experimental results revealed a considerable decline in creep rupture properties and a reduction in elongation for the specimens with sliver compared to their counterparts without sliver.

Yu et al.[76] also simulated the influence of different orientations of sliver defects on the creep-rupture life of a CMSX-4 superalloy under the same conditions (980 °C/250 MPa). As illustrated in Fig. 21(a), the simulation results demonstrate that as the misorientation of the sliver respect to the matrix increases, the creep life of the specimen decreases. When the misorientation is within the range of 0°–5°, its impact on the creep life is relatively small. For a misorientation of 5°, the creep life only decreases by 6% compared to that with a misorientaion of 0°. However, when the misorientation reaches 15°, there is a considerable decline in creep life, with a reduction of 47%. Using Origin software, they also fitted experimental and simulated data. They adopted an 80% standard for creep fracture life, to determine the damage tolerance of slivers. The fitting results, illustrated by the red line in Fig. 21(b), suggest that, for the nickel-based single crystal superalloy CMSX-4, under conditions of 980 °C/250 MPa, the damage tolerance of sliver is around 8°.

Li et al.[118] studied the effect of misorientation on the fatigue life of a DD5 single crystal superalloy. They reported that with an increase in misorientation angle, the fatigue life decreases. Furthermore, the orientation sensitivity of fatigue life is affected by stress level, and it is more sensitive to misorientation at a low stress. The results of fatigue test are presented in Fig. 22. A total of 17 valid data points were collected, with the exception of one from Group A subjected to a load of 640 MPa, which was excluded due to specimen damage resulting from improper handling. Overall, it is observed that the fatigue life of Group A, characterized by a smaller misorientation (5°), exceeds that of Group B, which has a

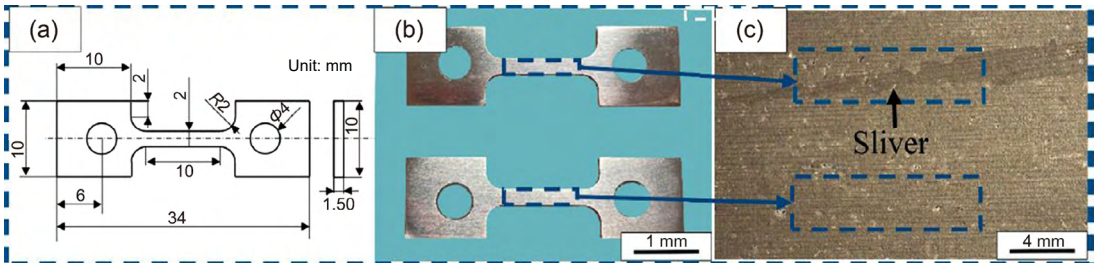

Fig. 19: Schematic diagram of the creep-rupture test specimens (a), creep-rupture specimens with and without sliver defects (b), and morphology of the sliver grain in the gauge section (c)[76]

Fig. 20: EBSD results for creep-rupture specimens: (a) without sliver; (b) with sliver[76]

Table 3: Creep-rupture properties of samples with and without sliver grains after heat treatment at 980 °C/250 MPa[76]

Sample No.	Rupture life (h)	Elongation (%)	Area reduction (%)
1 (without sliver)	143.35	16.00	9.98
2 (with sliver)	105.55	5.20	5.88

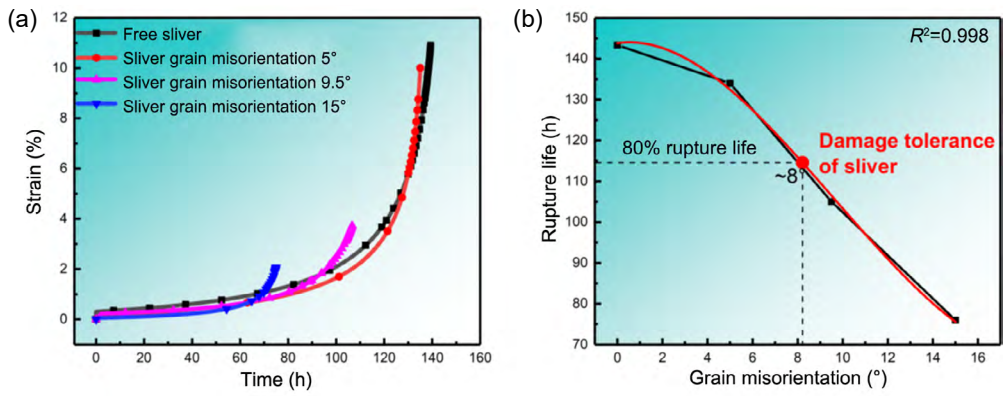

Fig. 21: Simulation results of creep-rupture life in the specimens with slivers of different orientations (a), and fitting results of sliver damage tolerance (b)[76]

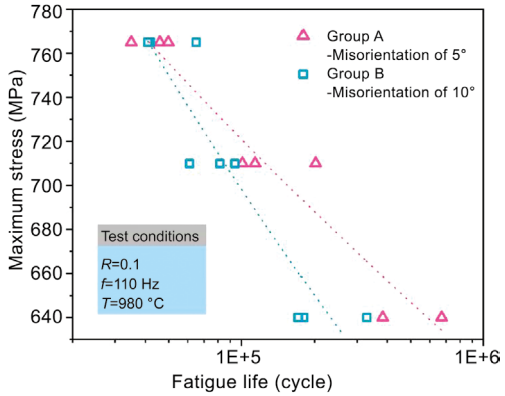

Fig. 22: Fatigue life of DD5 single crystal superalloy with maximum stress and misorientation[118]

relatively larger misorientation (10°). The data indicates that the sensitivity of fatigue life to orientation is affected by the stress level. Specifically, fatigue life demonstrates greater sensitivity to orientation at lower stress levels of 710 MPa and 640 MPa, while this sensitivity diminishes at 765 MPa. This implies that fatigue anisotropy is not notable within the investigated misorientation scope when the plastic activity is enhanced under a high load[118]. However, considering that the stress applied to the actual turbine blades during operation of turbine engines is lower than the values presented in Fig. 22[124, 125], it can be concluded that the presence of any misorientation defects, specially the slivers, in the blade structure can greatly affect the fatigue properties of single crystal blades.

3.6 Sliver prevention

Unlike some other defects, specially freckles, for which criteria have been proposed to prevent their formation in single crystal superalloy castings[55, 113, 126-129], no technique or criterion has been suggested to completely eliminate the slivers from superalloy components. The formation and evolution mechanisms of this defect are intricate, which involve contraction stress, temperature field, casting geometry, crystal orientation, melt quality, other solidification defects, and so on. Eliminating the sliver defects is still a challenge for manufacturers. However, the presence of these defects in single crystal castings can be minimized by reducing or eliminating factors that facilitate sliver formation and evolution. For instance, it is essential to maintain strict control over the quality of the mould, particularly the inner surface, which should remain smooth and free of contaminants to avoid localized stress during the solidification process. Additionally, it is crucial to minimize oxide inclusions during the melting and pouring processes. This is directly dependent on the quality of both the mould and crucible[130-132], as well as the master alloy ingot. Moreover, controlling the curvature of solidification front during casting can reduce the intensification of local stress fields on dendrites and consequently the susceptibility to sliver formation. Szeliga et al.[133] utilized an internal thermal baffle between casting and central rod of a ceramic mould to control the liquidus isotherm shape during solidification of a Ni-based single crystal superalloy. They confirmed that the use of an internal thermal baffle led to a reduction in the curvature of the solidification front and a decrease in the transversal temperature gradient, resulting in improved dendrite growth compared to the mould without an internal baffle. Some other modifications can be effective to reduce the width of mushy zone and the inclination of solid-liquid interface. For example, optimization of process parameters[134], as well as the casting arrangement in a cluster mould[135], can be considered as these modifications. Application of other directional solidification techniques that refine the dendritic microstructure, such as downward directional solidification[36-39] and liquid metal cooling technique (LMC)[31, 32, 136-138], can potentially restrict the competitive growth of sliver dendrites and prevent their evolution throughout the castings. The main advantage of these processes over the conventional Bridgman technique is the provision of a stable thermal gradient and also the reduction of the curvature of the solidification front, which can significantly reduce grain defects in addition to improving the microstructure. The downward directional solidification method also has another advantage. In this technique, the movement of the solidification front is downward and the problem of density inversion in the mushy zone does not arise. Therefore, the risk of thermal convection and, as a result, the formation of freckle defects is eliminated in this process[39]. However, due to the process and economic limitations of the aforementioned techniques, the Bridgman technique is still the most widely used in the manufacture of single crystal superalloys.

4 Summaries

This study comprehensively reviewed the sliver defects in single crystal superlloys. The main conclusions can be summarized as follows:

(1) Slivers are a group of low-to-medium angle misoriented grains whose misorientation angle may be up to 18°. However, their misorientation angle has reported lower than 10° in most cases. These defects introduce a group of longitudinal low-angle grain boundaries in the casting structure.

(2) Contrary to some previous reports, nucleation mechanisms play no role in the formation of slivers from the melt. Dendrite deformation and dendrite fracture (fragmentation/tearing) are the main mechanisms for the sliver formation.

(3) Dendrite fracture or deformation is induced by non-uniform thermal stresses during solidification. Therefore, any factor that enhances local stress concentration on dendrites during solidification, can intensify the sliver formation. Accordingly, localized microstructural or geometric heterogeneities, including inclusions, pores, curved surfaces, platform transitions, grain selector regions, mould joints, mould walls, and freckle channels can be considered as the potential factors that promote the sliver initiation.

(4) Sliver formation has a deleterious effect on the creep life of the single crystal superalloys. In such a way, when the misorientation reaches 15°, creep life can decline up to 47%. Additionally, similar to low-angle grain boundaries, the damage tolerance of the slivers in single crystal superalloys can be considered around 8°.

(5) There is not a specific criterion to prevent the sliver formation and evolution. However, by optimizing process parameters and properly designing the solidification technique, as well as carefully controlling materials and equipment, the presence of these defects in the structure can be minimized.

Conflict of interest

The authors declare that they have no conflict of interest.

References

[1] McLean M, Webster G A, Nabarro F R N, et al. Nickel-base superalloys: Current status and potential. Philos. Trans. R. Soc. A: Phys. Eng. Sci., 1995, 351: 419–433.
[2] Morad A, Shash Y M. Nickel base superalloys used for aero engine turbine blades. In: Proc. The 16th International Conference on Applied Mechanics and Mechanical Engineering, Cairo, Egypt, 2014: 1–22.
[3] Wahl J B, Harris K. Advanced Ni base superalloys for small gas turbines. Can. Metall. Q., 2011, 50(3): 207–214.
[4] Hashizume R, Yoshinari A, Kiyono T, et al. Development of novel Ni-based single crystal superalloys for power-generation gas turbines. Mater. High Temp., 2007, 24(3): 163.
[5] Wu Y, Chen B Q, Liu W, et al. Progress in research and applications of additively manufactured nickel-based superalloy in aero-engines and gas turbines. J. Aeronaut. Mater., 2024, 44(1): 31–45.
[6] Prashar G, Thakur K, Singh S, et al. Superalloys for high-temperature applications: An overview. In: AIP Conference Proceedings, 2024, 2986(1).
[7] Versnyder F I, Shank M E. The development of columnar grain and single crystal high temperature materials through directional solidification. Mater. Sci. Eng., 1970, 6(4): 213–247.
[8] Fu H, Geng X. High rate directional solidification and its application in single crystal superalloys. Sci. Technol. Adv. Mater., 2001, 2(1): 197–204.
[9] Liu L, Huang T W, Zhang J, et al. Microstructure and stress rupture properties of single crystal superalloy CMSX-2 under high thermal gradient directional solidification. Mater. Lett., 2007, 61(1): 227–230.
[10] Kermanpur A, Varahraam N, Engilehei E, et al. Directional solidification of Ni base superalloy IN738LC to improve creep properties. Mater. Sci. Technol., 2000, 16(5): 579–586.
[11] Cetel A D, Duhl D N. Second generation columnar grain nickel-base superalloy. Superalloys, 1992: 287–296.
[12] Jiang W, Li P, Yao W, et al. The effect of porosity size on the high cycle fatigue life of nickel-based single crystal superalloy at 980 °C. Int. J. Fatigue, 2021, 147: 106191.
[13] Ganesan M, Dye D, Lee P. A technique for characterizing microsegregation in multicomponent alloys and its application to single-crystal superalloy castings. Metall. Mater. Trans. A, 2005, 36: 2191–2204.
[14] Zhou Y. Formation of stray grains during directional solidification of a nickel-based superalloy. Scr. Mater., 2011, 65(4): 281–284.
[15] D'souza N, Ardakani M G, Wagner A, et al. Morphological aspects of competitive grain growth during directional solidification of a nickel-base superalloy, CMSX4. J. Mater. Sci., 2002, 37: 481–487.
[16] Ma D, Wu Q, Bührig-Polaczek A. Some new observations on freckle formation in directionally solidified superalloy components. Metall. Mater. Trans. B, 2012, 43(2): 344–353.
[17] Shi Z X, Liu S Z, Li J. Sliver fomation mechanism of single crystal superalloy during directional solidification process. Hot Work. Technol., 2013, 42: 31–33. (In Chinese)
[18] Sangid M D, Sehitoglu H, Maier H J, et al. Grain boundary characterization and energetics of superalloys. Mater. Sci. Eng. A, 2010, 527(26): 7115–7125.
[19] Liu Z, Li M, Wang F, et al. Effects of rhenium and high-angle grain boundaries upon the elemental distribution and microstructure of Ni-based single-crystal superalloys. Mater. Charact., 2023, 196: 112655.
[20] Rajabi Nejad S, Seifollahi M, Abbasi S M, et al. Influence of withdrawal rate on as-cast microstructure and stress-rupture life of directionally solidified Rene80 superalloy. J. Adv. Mater. Process., 2022, 10(2): 29–38.
[21] Chen Q Z, Kong Y H, Jones C N, et al. Porosity reduction by minor additions in RR2086 superalloy. Scr. Mater., 2004, 51(2): 155–160.
[22] Zhao Y, He S, Li L. Application of hot isostatic pressing in nickel-based single crystal superalloys. Crystals, 2022, 12(6): 805.
[23] Zheng X G, Shi Y N, Lou L. Healing process of casting pores in a Ni-based superalloy by hot isostatic pressing. J. Mater. Sci. Technol., 2015, 31(11): 1151–1157.
[24] Roncery L M, Lopez-Galilea I, Ruttert B, et al. Influence of temperature, pressure, and cooling rate during hot isostatic pressing on the microstructure of an SX Ni-base superalloy. Mater. Des., 2016, 97: 544–552.
[25] Ruttert B, Ramsperger M, Roncery B, et al. Impact of hot isostatic pressing on microstructures of CMSX-4 Ni-base superalloy fabricated by selective electron beam melting. Mater. Des., 2016, 110: 720–727.

[26] Warnken N. Studies on the solidification path of single crystal superalloys. J. Phase Equilibria Diffus., 2016, 37: 100–107.
[27] Caron P, Khan T. Improvement of creep strength in a nickel-base single-crystal superalloy by heat treatment. Mater. Sci. Eng., 1983, 61(2): 173–184.
[28] Fuchs G E. Solution heat treatment response of a third generation single crystal Ni-base superalloy. Mater. Sci. Eng. A, 2001, 300(1–2): 52–60.
[29] Liu C, Yang W C, Cao K L, et al. New insights into the microstructural stability based on the element segregation behavior at γ/γ′ interface in Ni-based single crystal superalloys with Ru addition. J. Mater. Sci. Technol., 2023, 154: 232–240.
[30] Cao L, Liao D, Lu Y, et al. Heat transfer model of directional solidification by LMC process for superalloy casting based on finite element method. Metall. Mater. Trans. A, 2016, 47: 4640–4647.
[31] Zhang H, Pei Y, Li S, et al. Effect of process parameters on microstructures and properties of DZ125 superalloy solidified by LMC. Mater. Res. Innov., 2014, 18 (4): S4–385.
[32] Liu C, Shen J, Zhang J, et al. Effect of withdrawal rates on microstructure and creep strength of a single crystal superalloy processed by LMC. J. Mater. Sci. Technol., 2010, 26(4): 306–310.
[33] Liu G, Liu L, Zhang G J, et al. Microstructure and element segregation of Ni-base superalloy casting with radiation and liquid-metal cooling. Materials Science Forum, 2015, 816: 608–612.
[34] Wang H, Long H B, Sun M, et al. Effect of directional solidification methods on solid solution window in Ni-based single-crystal superalloy. J. Mater. Res. Technol., 2023, 24: 8307–8319.
[35] Elliott A J, Pollock T M, Tin S, et al. Directional solidification of large superalloy castings with radiation and liquid-metal cooling: A comparative assessment. Metall. Mater. Trans. A, 2004, 35: 3221–3231.
[36] Wang F, Ma D, Zhang J, et al. Solidification behavior of a Ni-based single crystal CMSX-4 superalloy solidified by downward directional solidification process. Mater. Charact., 2015, 101: 20–25.
[37] Wang F, Ma D, Zhang J, et al. Effect of solidification parameters on the microstructures of superalloy CMSX-6 formed during the downward directional solidification process. J. Cryst. Growth, 2014, 389: 47–54.
[38] Wang F, Ma D, Bogner S, et al. Comparative investigation of the downward and upward directionally solidified single-crystal blades of superalloy CMSX-4. Metall. Mater. Trans. A, 2016, 47: 2376–2386.
[39] Wang F, Ma D, Zhang J, et al. Investigation of segregation and density profiles in the mushy zone of CMSX-4 superalloys solidified during downward and upward directional solidification processes. J. Alloys Compd., 2015, 620: 24–30.
[40] Parsa A, Ramsperger M, Kostka A, et al. Transmission electron microscopy of a CMSX-4 Ni-base superalloy produced by selective electron beam melting. Metals (Basel), 2016, 6(11): 258.
[41] Wood P, Díaz-Lvarez J, Rusinek A, et al. Microstructure effects on the machinability of AM-produced superalloys. Crystals, 2023, 13(8): 1190.
[42] Fan Z, Levine L E, Allen A J, et al. Effect of heat treatment on the microstructural evolution of a nickel-based superalloy additive-manufactured by laser powder bed fusion. Acta Mater., 2018, 152: 200–214.
[43] Amouyal Y, Seidman D N. An atom-probe tomographic study of freckle formation in a nickel-based superalloy. Acta Mater., 2011, 59(17): 6729–6742.
[44] Long Z D, Liu X B, Yang W H, et al. Thermodynamic assessment of liquid composition change during solidification and its effect on freckle formation in superalloys. Mater. Sci. Eng. A, 2004, 386(1–2): 254–261.
[45] Ren N, Li J, Panwisawas C, et al. Thermal-solutal-fluid flow of channel segregation during directional solidification of single-crystal nickel-based superalloys. Acta Mater., 2021, 206: 116620.
[46] Tin S, Pollock T M, Murphy W. Stabilization of thermosolutal convective instabilities in Ni-based single-crystal superalloys: Carbon additions and freckle formation. Metall. Mater. Trans. A, 2001, 32: 1743–1753.
[47] Zhang Y J, Jia Y L, Zhou J X, et al. Effect of withdrawal rate on freckle formation of large-size directional solidified nickel-based superalloy blades. J. Mater. Res. Technol., 2024, 30: 1518–1530.
[48] Wang Z, Li J, Liu S Z, et al. Effects of withdrawal velocity and casting geometry on freckle formation of nickel-based single crystal superalloys. Metall. Mater. Trans. A, 2023, 54(4): 1223–1235.
[49] Ma D, Bührig-Polaczek A. The geometrical effect on freckle formation in the directionally solidified superalloy CMSX-4. Metall. Mater. Trans. A, 2014, 45(3): 1435–1444.
[50] Hong J P, Ma D X, Wang J, et al. Geometrical effect of freckle formation on directionally solidified superalloy CM247 LC components. J. Alloys Compd., 2015, 648: 1076–1082.
[51] Han D, Jiang W, Xiao J H, et al. Influence of geometric structure and feeding behavior of casting on freckle formation during directional solidification of a Ni-based single-crystal superalloy. Cryst. Res. Technol., 2021, 56(5): 2000197.
[52] Liu Y, Wang F, Ma D X, et al. Freckle prediction model incorporating geometrical effects for Ni-based single-crystal superalloy components. Acta Mater., 2024, 266: 119702.
[53] Han D, Jiang W G, Xiao J H, et al. Investigation on freckle formation and evolution of single-crystal nickel-based superalloy specimens with different thicknesses and abrupt cross-section changes. J. Alloys Compd., 2019, 805: 218–228.
[54] Meng X B, Li J G, Chen Z Q, et al. Effect of platform dimension on the dendrite growth and stray grain formation in a Ni-base single-crystal superalloy. Metall. Mater. Trans. A, 2013, 44: 1955–1965.
[55] Yang X, Ness D, Lee P D, et al. Simulation of stray grain formation during single crystal seed melt-back and initial withdrawal in the Ni-base superalloy CMSX4. Mater. Sci. Eng. A, 2005, 413: 571–577.
[56] Xu M, Zhang X L, Geng X Q, et al. Study on the formation and competitive growth mechanism of stray grains during spiral grain selector of nickel-based single crystal superalloy. Mater. Lett., 2021, 294: 129747.
[57] Zhao X, Liu L, Yu Z, et al. Influence of directional solidification variables on the microstructure and crystal orientation of AM3 under high thermal gradient. J. Mater. Sci., 2010, 45: 6101–6107.
[58] Huo M, Liu L, Yang W C, et al. Dendrite growth and defects formation with increasing withdrawal rates in the rejoined platforms of Ni-based single crystal superalloys. Vacuum, 2019, 161: 29–36.
[59] Ren N, Li J, Wang B J, et al. Design of variable withdrawal rate for superalloy single-crystal blade fabrication. Mater. Des., 2021, 198: 109347.
[60] Rezaei M, Kermanpur A, Sadeghi F. Effects of withdrawal rate and starter block size on crystal orientation of a single crystal Ni-based superalloy. J. Cryst. Growth, 2018, 485: 19–27.
[61] Ebrahimiyan H, Kermanpur A, Heydari A R, et al. On the formation of stray grains in directionally-solidified Ni-based superalloys with varying cross sections. Iran. J. Mater. Sci. Eng, 2017, 14: 12–24.
[62] Meng X, Li J, Zhu S, et al. Method of stray grain inhibition in the platforms with different dimensions during directional solidification of a Ni-base superalloy. Metall. Mater. Trans. A, 2014, 45: 1230–1237.

[63] Xu W, Wang F, Ma D, et al. Sliver defect formation in single crystal Ni-based superalloy castings. Mater. Des., 2020, 196: 109138.
[64] Huang Y, Shen J, Wang D, et al. Formation of sliver defect in Ni-based single crystal superalloy. Metall. Mater. Trans. A, 2020, 51(1): 99–103.
[65] Han D, Jiang W, Xiao J, et al. Investigating the evolution of freckles into sliver defects in Ni-based single-crystal superalloy castings. Mater. Today Commun., 2021, 27: 102350.
[66] Sun D, Liu L, Huang T, et al. Formation of lateral sliver defects in the platform region of single-crystal superalloy turbine blades. Metall. Mater. Trans. A, 2019, 50(3): 1119–1124.
[67] Huo M, Liu L, Yang W, et al. Formation of slivers in the extended cross-section platforms of Ni-based single crystal superalloy. Adv. Eng. Mater., 2018, 20(9): 1701189.
[68] Huang Y, Shen J, Wang D, et al. Evolution of sliver defect in Ni-based single crystal superalloy. Metall. Mater. Trans. A, 2020, 51(12): 6364–6372.
[69] Ma D, Wang F, Xu W, et al. Formation of sliver defects in single crystal castings of superalloys. Acta Met. Sin., 2019, 56(3): 301–310.
[70] Ma D X, Wang F, Xu W, et al. Study on sliver defects in single crystal castings of superalloys. Foundry, 2019, 68: 567–573. (In Chinese)
[71] Xia H, Yang Y, Feng Q, et al. Generation mechanism and motion behavior of sliver defect in single crystal Ni-based superalloy. J. Mater. Sci. Technol., 2023, 137: 232–246.
[72] Beech J, Jones H. Solidification processing. In: 4th Decennial International Conference on Solidification Processing, 1997.
[73] Al-Jarba K A, Fuchs G E. Effect of carbon additions on the as-cast microstructure and defect formation of a single crystal Ni-based superalloy. Mater. Sci. Eng. A, 2004, 373(1–2): 255–267, 2004.
[74] Aveson J W, Tennant P A, Foss B J, et al. On the origin of sliver defects in single crystal investment castings. Acta Mater., 2013, 61(14): 5162–5171.
[75] Yang Q, Zhu X, Wang F, et al. A study of sliver in C-shaped grain selectors during investment casting of single-crystal superalloy. Metals (Basel)., 2023, 13(6): 1102.
[76] Yu X, Xuan W D, Zhang S J, et al. An Insight into the creep failure mechanism of sliver defect in the second-generation nickel-based single crystal superalloy CMSX-4. Engineering Fracture Mechanics, 2024. http://doi.org/10.1016/j.engfracmech.2024.110307.
[77] Zhang C, Huang T, Hu H, et al. Evolution of sliver morphology in large-sized single-crystal superalloy blades. Mater. Lett., 2025, 138030.
[78] Zhou Y Z, Volek A, Green N R. Mechanism of competitive grain growth in directional solidification of a nickel-base superalloy. Acta Mater., 2008, 56(11): 2631–2637.
[79] Kurz W, Fisher D, Rappaz M. Fundamentals of solidification, 5th edition. Foundations Mater. Sci. Eng., 2023. http://doi.org/10.4028/b-v7b35q.
[80] Zhou Y, Sun X. Effect of solidification rate on competitive grain growth in directional solidification of a nickel-base superalloy. Sci. China Technol. Sci., 2012, 55: 1327–1334.
[81] Giamei A F, Kear B H. On the nature of freckles in nickel base superalloys. Metall. Trans., 1970, 1(8): 2185–2192.
[82] Copley S M, Giamei A F, Johnson S M, et al. The origin of freckles in unidirectionally solidified castings. Metall. Trans., 1970, 1(8): 2193–2204.
[83] Li Q, Shen J, Qin L, et al. Investigation on local cooling in reducing freckles for directionally solidified superalloy specimens with abruptly varying cross-sections. Mater. Charact., 2017, 130: 139–148.
[84] Huo M, Liu L, Yang W, et al. Formation of low-angle grain boundaries under different solidification conditions in the rejoined platforms of Ni-based single crystal superalloys. J. Mater. Res., 2019, 34(2): 251–260.
[85] Bussac A, Gandin C A. Prediction of a process window for the investment casting of dendritic single crystals. Mater. Sci. Eng. A, 1997, 237(1): 35–42.
[86] Ren N, Panwisawas C, Li J, et al. Solute enrichment induced dendritic fragmentation in directional solidification of nickel-based superalloys. Acta Mater., 2021, 215: 117043.
[87] Gu J P, Beckermann C, Giamei A F. Motion and remelting of dendrite fragments during directional solidification of a nickel-base superalloy. Metall. Mater. Trans. A, 1997, 28: 1533–1542.
[88] Wang Z, Li J, Liu S Z, et al. Investigation on freckle formation of nickel-based single crystal superalloy specimens with suddenly reduced cross section. J. Alloys Compd., 2022, 918: 165631.
[89] Aveson J W, Reinhart G, Goddard C J L, et al. On the deformation of dendrites during directional solidification of a nickel-based superalloy. Metall. Mater. Trans. A, 2019, 50(11): 5234–5241.
[90] Huo M, Liu L, Yang W. Dendrite deformation in the rejoined platforms of Ni-based single-crystal superalloys. Adv. Eng. Mater., 2023, 25(16): 2300385.
[91] Shenoy M M, Kumar R S, McDowell D L. Modeling effects of nonmetallic inclusions on LCF in DS nickel-base superalloys. Int. J. Fatigue, 2005, 27(2): 113–127.
[92] Yang S, Tian Q, Yang S, et al. Study on the nucleation mechanism of car-bonitrides on $LaAlO_3$ in GH4742 superalloy. J. Mater. Res. Technol., 2023, 26: 5309–5320.
[93] Moshtaghi M, Abbasi S M. Effect of vacuum degree in VIM furnace on mechanical properties of Ni-Fe-Cr based alloy. Trans. Nonferrous Met. Soc. China, 2012, 22(9): 2124–2130.
[94] Gao R, Wang L, Chen C, et al. Agglomeration behavior of alumina inclusions and calcium aluminate inclusions on molten nickel-based superalloy surface. J. Iron Steel Res. Int., 2023, 30(11): 2318–2327.
[95] Carney C. Origin of sliver defects in single crystal turbine blades. In: 4th Decennial International Conference on Solidification Processing, Ranmoor House, University of Sheffield, UK, 1997: 33–36.
[96] Jiang J, Yang J, Zhang T, et al. Microstructurally sensitive crack nucleation around inclusions in powder metallurgy nickel-based superalloys. Acta Mater., 2016, 117: 333–344.
[97] Anton D L, Giamei A F. Porosity distribution and growth during homogenization in single crystals of a nickel-base superalloy. Mater. Sci. Eng., 1985, 76: 173–180.
[98] Yue Q, Liu L, Yang W, et al. Influence of withdrawal rate on the porosity in a third-generation Ni-based single crystal superalloy. Prog. Nat. Sci. Mater. Int., 2017, 27(2): 236–243.
[99] Epishin A, Link T. Mechanisms of high-temperature creep of nickel-based superalloys under low applied stresses. Philos. Mag., 2004, 84(19): 1979–2000.
[100] Tian S, Jiang C, Zhang S, et al. Influence and analysis of defects on creep behaviors of a single crystal nickel-based superalloy. Mater. Sci. Eng. A, 2014, 613: 184–192.
[101] Tan Z, Wang X, Ge Z, et al. Dependence of deformation mechanisms on micro-pores in the fourth-generation single crystal superalloy during out-of-phase thermal-mechanical fatigue. Int. J. Fatigue, 2024, 180: 108086.
[102] Plancher E, Gravier P, Chauvet E, et al. Tracking pores during solidification of a Ni-based superalloy using 4D synchrotron microtomography. Acta Mater., 2019, 181: 1–9.
[103] Wang F, Ma D X. A high thermal gradient directional solidification method for growing superalloy single crystals. J. Mater. Process. Technol., 2014, 214(12): 3112–3121.

[104] Kim S H, Kim J M, Lee H J, et al. Effect of thermal gradient on solidification microstructure in the Ni-base single crystal superalloy CMSX10. In: Defect and Diffusion Forum, 2008, 273: 361–366.
[105] Zhang Y, Li J. Characterization of the microstructure evolution and microsegregation in a Ni-based superalloy under super-high thermal gradient directional solidification. Mater. Trans., 2012, 53(11): 1910–1914.
[106] Zhao Y, Zhang M, Yang L, et al. Effect of the withdrawal rate on the microstructure and thermal durability of a third-generation single crystal superalloy. Prog. Nat. Sci. Mater. Int., 2021, 31(3): 493–500.
[107] Liu G, Liu L, Cheng A, et al. Influence of withdrawal rate on the microstructure of Ni-base single-crystal superalloys containing Re and Ru. J. Alloys Compd., 2011, 509(19): 5866–5872.
[108] Long F, Yoo Y S, Seo S M, et al. Effect of Re addition and withdrawal rate on the solidification behavior of directionally solidified superalloy AM3. J. Mater. Sci. Technol., 2011, 27(2): 101–106.
[109] Li Q, Shen J, Qin L, et al. Investigation on freckles in directionally solidified CMSX-4 superalloy specimens with abrupt cross section variation. J. Alloys Compd., 2017, 691: 997–1004.
[110] Dong Y W, Li X L, Zhao Q, et al. Geometrical modeling to improve the accuracy of drilled cooling holes on turbine blades. Int. J. Adv. Manuf. Technol., 2017, 93: 4409–4428.
[111] Ma D. Freckle formation during directional solididicatiopn of complex castings of superalloys. Acta Met. Sin, 2016, 52 (4): 426–436.
[112] Auburtin P B L. Determination of the influence of growth front angle on freckle formation in superalloys. Doctoral Dissertation, Vancouver: University of British Columbia, 1998.
[113] Ortiz V, Antonio J. Preventing solidification defects in large superalloy castings used in advanced electric power systems. Doctoral Dissertation, West Virginia University, 2010. https://api.semanticscholar.org/CorpusID:137516541.
[114] Tang H, Guo H. Effect of grain defects on the mechanical behavior of nickel-based single crystal superalloy. Int. J. Mater. Res., 2017, 108(3): 163–172.
[115] Dreshfield R L. Defects in nickel-base superalloys. JOM, 1987, 39(7): 16–21.
[116] Rae C M F, Reed R C. Primary creep in single crystal superalloys: Origins, mechanisms and effects. Acta Mater., 2007, 55(3): 1067–1081.
[117] Matan N, Cox D C, Carter P, et al. Creep of CMSX-4 superalloy single crystals: Effects of misorientation and temperature. Acta Mater., 1999, 47(5): 1549–1563.
[118] Li P, Cox D C, Carter P, et al. Effect of misorientation on the fatigue life of nickel-base single crystal superalloy DD5 at 980 °C. Int. J. Fatigue, 2021, 153: 106479.
[119] Li J R, Zhao J Q, Liu S Z, et al. Effects of low angle boundaries on the mechanical properties of single crystal superalloy DD6. Superalloys, 2008, 2008: 443–451.
[120] Zhang J, Huang T, Liu L, et al. Advances in solidification characteristics and typical casting defects in nickel-based single crystal superalloys. Acta Met. Sin, 2015, 51(10): 1163–1178. (In Chinese)
[121] Rong P, Wang N, Wang L, et al. The influence of grain boundary angle on the hot cracking of single crystal superalloy DD6. J. Alloys Compd., 2016, 676: 181–186.
[122] Huang M, Zhou L, Liu Z, et al. Misorientation related microstructure at the grain boundary in a nickel-based single crystal superalloy. Mater. Sci. Eng. A, 2015, 640: 394–401.
[123] Svensson L E, Dunlop G L. Growth of intergranular creep cavities. Int. Met. Rev., 1981, 26(1): 109–131.
[124] Wang R, Jiang K, Jing F, et al. Thermomechanical fatigue failure investigation on a single crystal nickel superalloy turbine blade. Eng. Fail. Anal., 2016, 66: 284–295.
[125] Guedou J Y, Honnorat Y. Thermomechanical fatigue of turbo-engine blade superalloys. In: Thermomechanical Fatigue Behavior of Materials, ASTM International, 1993.
[126] Auburtin P, Wang T, Cockcroft S L, et al. Freckle formation and freckle criterion in superalloy castings. Metall. Mater. Trans. B, 2000, 31(4): 801–811.
[127] Beckermann C, Gu J P, Boettinger W J. Development of a freckle predictor via Rayleigh number method for single-crystal nickel-base superalloy castings. Metall. Mater. Trans. A, 2000, 31(10): 2545–2557.
[128] Shukla A, DiDomizio R, Meshkov A, et al. Freckle formation propensity criterion for new superalloy design. In: International Symposium on Superalloys, Journal of Physics: Conference Series (JPCS), 2024: 186–194.
[129] Liu Y, Wang F. A novel prediction model of the freckle defects for single-crystal superalloy blades. Journal of Physics: Conference Series, 2024, 2686(1): 12013.
[130] Akmal M, Kang D S, Lee H, et al. Understanding the metal-mold interfacial reactions during directional solidification of superalloys using Al_2O_3-rich ceramic mold. J. Alloys Compd., 2024, 994: 174735.
[131] Zhang L, Chen J, Xing W, et al. Investigation of oxide inclusion films in cast superalloy impeller. Journal of Physics: Conference Series, 2024, 2808(1): 12016.
[132] Gao X, Zhang L, Qu X, et al. Effect of interaction of refractories with Ni-based superalloy on inclusions during vacuum induction melting. Int. J. Miner. Metall. Mater., 2020, 27: 1551–1559.
[133] Szeliga D, Kubiak K, Sieniawski J. Control of liquidus isotherm shape during solidification of Ni-based superalloy of single crystal platforms. J. Mater. Process. Technol., 2016, 234: 18–26.
[134] Szeliga D. Effect of processing parameters and shape of blade on the solidification of single-crystal CMSX-4 Ni-based superalloy. Metall. Mater. Trans. B, 2018, 49: 2550–2570.
[135] Lian Y, Li D, Zhang K. Effects of the location of a cast in the furnace on flatness of the solidification front in directional solidification. J. Cryst. Growth, 2016, 451: 33–41.
[136] Li Y, Liu L, Huang T, et al. Simulation of stray grain formation in Ni-base single crystal turbine blades fabricated by HRS and LMC techniques. China Foundry, 2017, 14(2): 75–79.
[137] Yan X, Wang R, Xu Q, et al. Numerical simulation and experimental casting of nickel-based single-crystal superalloys by HRS and LMC directional solidification processes. High Temp. Mater. Process., 2017, 36(4): 327–337.
[138] Steuer S, Villechaise P, Pollock T M, et al. Benefits of high gradient solidification for creep and low cycle fatigue of AM1 single crystal superalloy. Mater. Sci. Eng. A, 2015, 645: 109–115.